Advances in Colloid and Interface Science 206 (2014) 382–398

Contents lists available at ScienceDirect

Advances in Colloid and Interface Science

journal homepage: www.elsevier.com/locate/cis

Simultaneous spreading and evaporation: Recent developments

Sergey Semenov [a], Anna Trybala [a], Ramon G. Rubio [b], Nina Kovalchuk [a,c], Victor Starov [a,*], Manuel G. Velarde [d]

[a] Department of Chemical Engineering, Loughborough University, Loughborough LE 11 3TU, UK
[b] Department of QuímicaFísica I, Universidad Complutense, 28040 Madrid, Spain
[c] Institute of Biocolloid Chemistry, 03142 Kiev, Ukraine
[d] Instituto Pluridisciplinar, Paseo Juan XXIII, 1, Madrid 28040, Spain

ARTICLE INFO

Available online 4 September 2013

Keywords:
Wetting
Evaporation
Hysteresis of contact angle
Universal behaviour
Nanofluids
Surfactant solutions

ABSTRACT

The recent progress in theoretical and experimental studies of simultaneous spreading and evaporation of liquid droplets on solid substrates is discussed for pure liquids including nanodroplets, nanosuspensions of inorganic particles (nanofluids) and surfactant solutions. Evaporation of both complete wetting and partial wetting liquids into a nonsaturated vapour atmosphere are considered. However, the main attention is paid to the case of partial wetting when the hysteresis of static contact angle takes place. In the case of complete wetting the spreading/evaporation process proceeds in two stages. A theory was suggested for this case and a good agreement with available experimental data was achieved. In the case of partial wetting the spreading/evaporation of a sessile droplet of pure liquid goes through four subsequent stages: (i) the initial stage, spreading, is relatively short (1–2 min) and therefore evaporation can be neglected during this stage; during the initial stage the contact angle reaches the value of advancing contact angle and the radius of the droplet base reaches its maximum value, (ii) the first stage of evaporation is characterised by the constant value of the radius of the droplet base; the value of the contact angle during the first stage decreases from static advancing to static receding contact angle; (iii) during the second stage of evaporation the contact angle remains constant and equal to its receding value, while the radius of the droplet base decreases; and (iv) at the third stage of evaporation both the contact angle and the radius of the droplet base decrease until the drop completely disappears. It has been shown theoretically and confirmed experimentally that during the first and second stages of evaporation the volume of droplet to power 2/3 decreases linearly with time. The universal dependence of the contact angle during the first stage and of the radius of the droplet base during the second stage on the reduced time has been derived theoretically and confirmed experimentally. The theory developed for pure liquids is applicable also to nanofluids, where a good agreement with the available experimental data has been found. However, in the case of evaporation of surfactant solutions the process deviates from the theoretical predictions for pure liquids at concentration below critical wetting concentration and is in agreement with the theoretical predictions at concentrations above it.

Contents

* Corresponding author. Tel.: +44 1509 222508; fax: +44 1509 223923.
E-mail address: V.M.Starov@lboro.ac.uk (V. Starov).

0001-8686/$ – see front matter.
http://dx.doi.org/10.1016/j.cis.2013.08.006

1. Introduction. Kinetics of wetting of pure liquids and contact angle hysteresis

It is well established that kinetics of wetting and spreading of pure liquids in the absence of body forces is completely determined by the surface forces action in a vicinity of the three phase contact line [1]. There are numerous publications on the measurements of surface forces and their applications (see for example [1–6]). A manifestation of surface forces action is the presence of disjoining/conjoining pressure, which was suggested to refer as "Derjaguin's pressure" to recognise B. Derjaguin's contribution to the area [7].

A theory of kinetics of spreading of droplets in the case of complete wetting has been suggested some time ago and experimentally verified [1,8,9]. Comparison with available experimental data of the theoretical predictions showed both a qualitative and a quantitative agreement [1]. It is important to notice for the discussion below that in the case of complete wetting there is no contact angle hysteresis: a liquid droplet being deposited on a solid substrate spreads out completely, a dynamic contact angle, $\theta(t)$, decreases over time to zero value. Isotherm of Derjaguin's pressure in the case of complete wetting is schematically shown by curve 1 in Fig. 1.

Isotherms of type 1 are observed in cases of complete wetting, for example, oil on quartz, glass, and metal surfaces [2]. Isotherms for the partial wetting (curve 2 in Fig. 1) are observed for water and aqueous electrolyte solutions on a wide range of solid surfaces, for example on quartz, glass, and metal surfaces [2]. Liquid films with a thickness $h < h_{min}$ are referred to as α — films, which are thermodynamically stable. Much thicker films with $h > h_{max}$ are referred to as meta-stable β-films. Flat liquid films in between $h_{min} < h < h_{max}$ are unstable.

Situation differs in the case of partial wetting: a liquid droplet after a deposition spreads out until some critical contact angle is reached, which is referred to as a static advancing contact angle, θ_a. After that a macroscopic motion does not proceed any longer, though a slow microscopic spreading in front of the meniscus in the region of thin liquid films still goes on [1,10]. In the case of decreasing of volume, for example due to evaporation, droplet will start receding only after a static receding contact angle, θ_r, is reached. The latter phenomenon is referred to as a contact angle hysteresis and it is present in the case of partial or non-wetting. Derjaguin's pressure in the case of partial wetting is schematically shown by curve 2 in Fig. 1. Note that the equilibrium contact angle, θ_e, in the case of partial wetting on smooth homogeneous solid substrate can be expressed approximately as $\cos\theta_e \approx 1 - \frac{S_- - S_+}{\infty\gamma}$ (see Fig. 1), where γ is a liquid–air interfacial tension, $S_+ - S_- = \int_{h0}^{\infty} \Pi(h)dh$, and Π is the disjoining pressure. See [1] for more details.

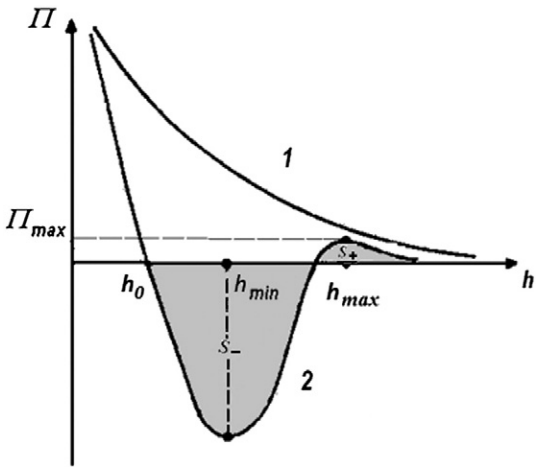

Fig. 1. Two types of isotherms of disjoining pressure: 1 — complete wetting case, 2 — partial wetting case.

Explanation of a hysteresis of contact angle on smooth homogeneous solid substrates is related to the s-shape isotherm of Derjaguin's pressure [1,7] (curve 2 in Fig. 1). This explanation is qualitatively described below.

Let us consider the static hysteresis of contact angle in the case of partial wetting in a flat capillary (Fig. 2). Consideration of the advancing contact angle in the case of droplet is given in [7]. The capillary is in contact with a reservoir, where the pressure, $P_a - P_e$, is kept, that is the pressure in the reservoir is lower than the atmospheric pressure, P_a, by the value of the excess pressure, P_e.

If we increase the pressure under the meniscus then the meniscus does not move but changes its curvature to compensate the excess pressure and, as a consequence, the contact angle increases accordingly. The meniscus does not move until some critical pressure and critical contact angle, θ_a, are reached. After further increase in pressure the meniscus starts to advance. A similar phenomenon takes place if we decrease the pressure under the meniscus: it does not recede until a critical pressure and corresponding critical contact angle, θ_r, are reached. The latter means that in the whole range of contact angles, $\theta_r < \theta < \theta_a$, the meniscus does not move macroscopically. The presence of the contact angle hysteresis shows that the actual equilibrium contact angle is very difficult to determine experimentally. It is the reason why only θ_a or θ_r is usually reported.

It is obvious that on the smooth homogeneous solid substrate only one contact angle corresponds to the equilibrium position and all the other positions are not equilibrium ones. Explanation of the hysteresis of contact angle on smooth homogeneous solid substrates is based on the s-shaped isotherm of Derjaguin's pressure in the case of partial wetting (curve 2, Fig. 1). Note, there are two branches on the isotherm corresponding to stable films (curve 2, Fig. 1). The thin α-films are thermodynamically stable ones, whereas thick β-films are metastable. This particular shape of isotherm determines a very special shape of the transition zone in the case of equilibrium meniscus [1,7]. In the case of increasing of the pressure behind the meniscus (Fig. 2a) a detailed consideration [1,7] of the transition zone shows: close to the "dangerous" point marked in Fig. 2a, the slope of the profile becomes steeper with increasing pressure. In region 3 in Fig. 2a there is a zone of flow. Viscous resistance in this region is very high because of very small thickness of the film, that is why the advancing of the meniscus proceeds very slowly. After some critical pressure behind the meniscus is reached, the slope at the "dangerous" point reaches $\pi/2$ and the fast "caterpillar" motion starts as shown in Fig. 2a. (See [11] for more details).

In the case of decreasing the pressure behind the meniscus the event proceeds according to Fig. 2b. In this case again up to some critical

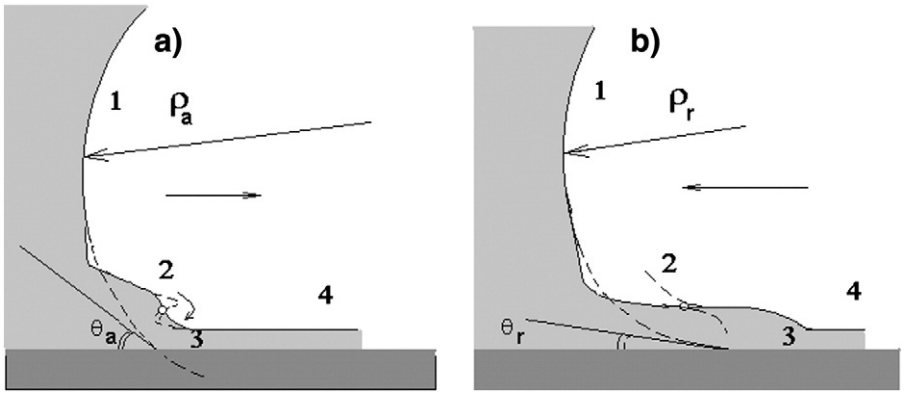

Fig. 2. Hysteresis of contact angle in capillaries in the case of partial wetting (s-shaped isotherm of Derjaguin's pressure). (a) — advancing contact angle. 1 — a spherical meniscus of radius ρ_a, 2 — transition zone with a "dangerous" marked point (see explanation in the text), 3 — zone of flow, 4 — flat film. Close to the marked point a dashed line shows the profile of the transition zone just after the contact angle reaches the critical value θ_a, a beginning of a "caterpillar motion". (b) — receding contact angle. 1 — a spherical meniscus of radius $\rho_r < \rho_a$, 2 — transition zone with a "dangerous" marked point (see explanation in the text), 3 — zone of flow, 4 — flat film. Close to the marked point dashed lines show the profile of the transition zone just after the contact angle reaches the critical value θ_r.

pressure the slope in the transition zone close to the "dangerous" marked point becomes more and more flat. In region 3 in Fig. 2b there is a zone of flow. Viscous resistance in this region again is very high, that is why the receding of the meniscus proceeds very slowly. After some critical pressure behind the meniscus is reached the profile in the vicinity of the "dangerous" point shows a discontinuous behaviour, which is obviously impossible. That means the meniscus will start to slide along thick β-film [1,7]. That is, the meniscus will move relatively fast leaving behind a thick β-film. The latter phenomenon (the presence of a thick β-film behind the receding meniscus of aqueous solutions in quartz capillaries) has been discovered experimentally [12–14] and supports our arguments explaining *static* contact angle hysteresis on smooth homogeneous substrates (see [11] for more details).

The critical film thickness in the case of static advancing contact angle presented in Fig. 2a is around 10 nm. However, in the case of the static receding contact angle (Fig. 2B) the critical thickness is considerably bigger, around 100 nm. Hence, according to this mechanism the solid surface roughness less than 10 nm does not have any influence on both static advancing and static receding contact angles and static receding contact angle is less sensitive to the roughness of the solid substrate.

In the process of deposition of droplets the latter reach the final position after the contact angle reaches the static advancing contact angle, as discussed in details in [7] via analysis of events in a vicinity of the apparent three phase contact line. This consideration revealed that the static advancing contact angle in the case of droplets substantially differs from the corresponding static advancing contact angle in the capillaries: in the case of droplets the latter is not a unique property of droplet–solid substrate system but depends on the droplet volume. It was shown that the advancing contact angle of droplet increases with a decrease of the droplet volume. This theoretical conclusion was directly confirmed experimentally in [15–17].

Thus, as discussed above, consideration of kinetics of spreading in the case of partial wetting is not as straightforward as in the case of complete wetting, because of a complicated form of s-shaped Derjaguin's pressure isotherm (curve 2, Fig. 1) and this area is to be developed. Far more difficult is the application of Derjaguin's pressure to the case of kinetics of wetting and spreading on rough and non-homogeneous solids, therefore this topic is to be investigated further. A real physical explanation of wetting and spreading in the case of hydrophobic substrates is to be developed.

2. Kinetics of simultaneous spreading and evaporation

Both diffusion-limited and phase change-limited models of evaporation are widely used in literature. Among others Ajaev et al. [18] and Rednikov and Colinet [19] applied phase change-limited models of evaporation.

Ajaev et al. [18] studied both static and dynamic values of the apparent contact angle for gravity-driven flow of a volatile liquid down of a heated inclined plane. The authors investigated macroscopic boundary conditions which could be used with a conventional continuum approach and agreed with the microscale phenomena at the contact line. They found the profile of the liquid–vapour interface and determined the dependence of the macroscopic contact angle on the temperature of the contact line and the velocity of its motion. The interface profile in the region was determined by a disjoining pressure action. It was found that the curvature of the interface at that transition region is very high.

Rednikov and Colinet [19] studied the microstructure of a contact line formed by a liquid and its pure vapour for a perfectly wetted superheated smooth substrate with a disjoining pressure in the form of a positive inverse cubic law. They took a spreading coefficient as an independent parameter in their study. Results show that the regime of a truncated liquid microfilm on a solid surface can be thermodynamically more stable than the regime of an extended microfilm (covering the whole solid surface), even if the spreading coefficient is still positive (perfect wetting).

Below we consider a case of diffusion-limited evaporation. Other models of evaporation (in particular phase change-limited evaporation) are discussed in more details in the section "Evaporation of microdroplets of pure liquids".

2.1. Singularities in a vicinity of the three phase contact line

Two mathematical singularities have to be overcome, which arise in the case of theoretical consideration of simultaneous spreading and evaporation of liquid droplets [11]: the first point is associated with the well-known problem of a singularity at the moving three phase contact line (a singularity of the viscous stress caused by an incompatibility of non-slip condition on the solid substrate and free surface at the liquid–air interface in a vicinity of the three phase contact line), the second problem is associated with the specific behaviour of the evaporation flux at the perimeter of the droplet. Again, this singularity is caused by an incompatibility of boundary conditions at the liquid–air interface with those at the solid–liquid and the solid–air interface at the three phase contact line and results in artificial infinite increase of the evaporation flux in a vicinity of the three phase contact line [20,21]. Both singularities can be overcome by introducing the Derjaguin's (disjoining/conjoining) pressure into the model, which dominates in a vicinity of the apparent three-phase contact line [11,22–25]. Note that the latent heat of vaporization and Marangoni convection [26] inside

the droplets in the course of droplet evaporation has also to be taken into account.

2.2. Dependence of the evaporation flux on the droplet size

Theoretical and computer simulation studies [26–31] give the following equation for the evaporation rate of a sessile droplet:

$$\frac{dV}{dt} = -\beta F(\theta) L, \tag{1a}$$

where according to [32]

$$\beta = 2\pi \frac{DM}{\rho}\left(c\left(T_{surf}\right) - Hc(T_\infty)\right)$$

or simply as

$$\frac{dV(t)}{dt} = -\alpha L(t), \quad \alpha = \beta F(\theta), \tag{1b}$$

where V is the droplet volume, t is the time, D, ρ, and M are the vapour diffusivity in the air, the density of the liquid and the molar mass, respectively; H is the humidity of the ambient air, and T_{surf} is the average temperature of the droplet–air interface, $T_{surf} = \frac{1}{s}\int_S T_s(s,t)ds$ [32], where S is the liquid–air interface, $T_s(s,t)$ is a temperature of the surface at the position s on the interface and T_∞ is the temperature of the ambient air; $c(T_{surf})$ and $c(T_\infty)$ are the molar concentrations of saturated vapour at the corresponding temperature; $F(\theta)$ is a function of contact angle θ, which equals 1 at $\theta = {}^{\pi}/_{2}$ [27]. According to [27] there is a simple polynomial fitting of this function in two ranges of contact angle as follows $F(\theta) = (0.6366 \cdot \theta + 0.09591 \cdot \theta^2 - 0.06144 \cdot \theta^3)/\sin\theta$ if $\theta < \pi/18$ and $F(\theta) = (0.00008957 + 0.6333 \cdot \theta + 0.116 \cdot \theta^2 - 0.08878 \cdot \theta^3 + 0.01033 \cdot \theta^4)/\sin\theta$ if $\theta > \pi/18$. Eq. (1a) was deduced for the model of evaporation which takes into account diffusion only of the vapour in the surrounding air. In the case of θ independent on L (the first stage of evaporation) Eq. (1a) gives the evaporation rate directly proportional to the radius of the droplet base, L.

It has been shown [32,33] that proportionality of the total evaporation flux, J, to the droplet perimeter has nothing to do with a distribution of the local evaporation flux, j, over the droplet surface in the case of sufficiently big droplets (bigger than 1 μm). Let us reproduce the derivation of that statement by considering a stationary diffusion equation for vapour in air:

$$\frac{1}{r}\frac{\partial}{\partial r}\left(r\frac{\partial c}{\partial r}\right) + \frac{\partial^2 c}{\partial z^2} = 0, \tag{2}$$

where r and z are the radial and vertical co-ordinates, respectively (see Fig. 3); and c is the molar vapour concentration.

The local normal flux, j, from the surface of the droplet is

$$j = -D\frac{\partial c}{\partial \vec{n}}\bigg|_{z=h(r)} = -D\left(\frac{\partial c}{\partial r}\bigg|_{z=h(r)} n_r + \frac{\partial c}{\partial z}\bigg|_{z=h(r)} n_z\right), \tag{3}$$

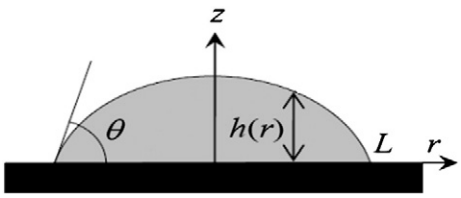

Fig. 3. A droplet on a solid substrate.

where $\vec{n} = (n_r, n_z)$ are a unit vector normal to the liquid–air interface (pointing into the air), and its radial and vertical components, respectively; and $h(r)$ is the height of the droplet surface. Let us introduce dimensionless variables using the same symbols as the original dimensional ones but with an over-bar: $\bar{z} = z/L$, $\bar{r} = r/L$, $\bar{c} = c/c_\infty$, $\bar{h} = h/L$, where L is the radius of the droplet base, c_∞ is the molar concentration of the vapour in the ambient air. Then Eq. (3) can be rewritten as:

$$j = -D\frac{\partial c}{\partial \vec{n}}\bigg|_{z=h(r)} = -\frac{Dc_\infty}{L}\left(\frac{\partial \bar{c}}{\partial \bar{r}}\bigg|_{\bar{z}=\bar{h}(\bar{r})} n_r + \frac{\partial \bar{c}}{\partial \bar{z}}\bigg|_{\bar{z}=\bar{h}(\bar{r})} n_z\right) = \frac{Dc_\infty}{L}A(\bar{r},\bar{z}), \tag{4}$$

where $A(\bar{r},\bar{z}) = \left(\frac{\partial \bar{c}}{\partial \bar{r}}\Big|_{\bar{z}=\bar{h}(\bar{r})} n_r + \frac{\partial \bar{c}}{\partial \bar{z}}\Big|_{\bar{z}=\bar{h}(\bar{r})} n_z\right)$. Hence, the total flux is

$$J = 2\pi\int_0^L rj\sqrt{1+\left(\frac{\partial h}{\partial r}\right)^2}\,dr = 2\pi LDc_\infty\int_0^1 \bar{r}A(\bar{r},\bar{z})\sqrt{1+\left(\frac{\partial \bar{h}}{\partial \bar{r}}\right)^2}\,d\bar{r}. \tag{5}$$

The latter two equations show that the total flux, $J \sim L$, and the local flux $j \sim 1/L$. Note, those properties do not depend on the distribution of the local evaporation flux, j, over the droplet surface. The latter conclusions agree with the previous consideration by Cazabat et al. [34]. Note, that those properties are valid only in the case of diffusion controlled evaporation, that is, for a droplet bigger than 1 μm (see below).

3. Thermal phenomena at evaporation

Dunn et al. [35] solved the coupled problem of vapour diffusion and heat transfer for the evaporation of sessile droplets of different liquids on substrates with different thermal properties. They demonstrated both experimentally and numerically that the heat conductivity of the substrate strongly influences the evaporation rate. Decreasing the heat conductivity of the substrate causes the decrease of the evaporation rate.

Experiments by David et al. [36] have also shown that temperature in the bulk of a sessile evaporating droplet substantially depends on the thermal properties of the substrate and the rate of evaporation. Their measurements (Fig. 4) clearly show that temperature of an evaporating droplet is different from the ambient temperature and almost constant in the course of evaporation. The latter is used below.

In [32] the dependence of the total vapour flux, J, on the radius of the droplet base, L, and the contact angle, θ was investigated using numerical simulations. All calculations were performed with effects of both local heat of vaporization (LHV) and Marangoni convection (MC) included. The results were obtained for substrates made of materials of various thermal conductivity and compared to those calculated for the

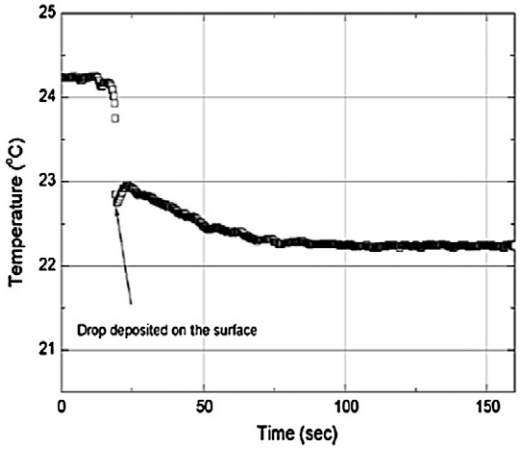

Fig. 4. Evolution of temperature inside the droplet after water droplet is deposited on PTFE substrate. Redrawn from [36].

isothermal cases by Hu and Larson [33] and Schonfeld et al. [37]. In the case of highly heat conductive solid support (copper) the difference between the present simulations and the results from [33,37] for isothermal case do not exceed 3% [32]. The latter is because of a small temperature change at the droplet surface, which is close to isothermal conditions. However, if other materials are used with lower heat conductivity (down to the heat conductivity of air), then the evaporation flux is substantially reduced as compared with the isothermal case [32]. Such flux reduction is connected to the noticeable temperature decrease of the droplet surface.

In [32] the mean temperature of the droplet surface: $T_{surf} = \frac{1}{S}\int_S T_s ds$ was introduced, where S is the surface area of the evaporating droplet. The dimensionless total flux $J/J_{\pi/2}(L,T_{surf})$ was plotted in [32], where $J_{\pi/2}$ is the total flux in the case then the contact angle is equal to π/2. All calculated total fluxes [32] for all substrates turned out to be on one universal dependence of total vapour flux, J, versus contact angle, θ: This universal dependency coincides with the dependency for the isothermal case if T_{surf} is used as a temperature of the droplet–air interface. The latter shows that the variation of the surface temperature is the major phenomenon influencing the evaporation rate (Figs. 5 and 6). Note that $J_{\pi/2}$ in Fig. 5 was calculated by taking the temperature on the droplet surface to be equal to the temperature of the substrate, $T_{substr} = T_\infty + 5\ K$, whereas in Fig. 6 the average temperature, T_{surf}, was used instead.

3.1. Distribution of the density of vapour flux over the droplet surface

The previous consideration shows that the proportionality of total evaporation flux, J, to the radius of the droplet base, L, and accordingly its proportionality to the perimeter of the droplet do not necessarily mean that evaporation occurs mostly at the droplet perimeter.

Meanwhile a number of researches in the field showed that in the case of contact angles $\theta < 90°$ the evaporation indeed is more intensive in a vicinity of the three-phase contact line. Several different principles were utilised in order to explain this phenomenon: (i) non-uniform distribution of vapour flux over the droplet surface due to the diffusion controlled process of vapour transfer to the ambient air [20,21,38]; (ii) action of Derjaguin's (disjoining/conjoining) pressure at the three-phase contact line [11,18,22–24]; (iii) evaporative cooling of the liquid–gas interface (due to latent heat of vaporization) and formation of the temperature field leading to a comparatively more intensive evaporation at the three-phase contact line [39].

Starov and Sefiane [39] suggested a physical mechanism of redistribution of evaporation flux which is controlled by the temperature field rather than by the process of vapour diffusion into air. According to their model, there is convection in the ambient air, so that vapour diffusion occurs only in a narrow boundary layer of thickness, δ.

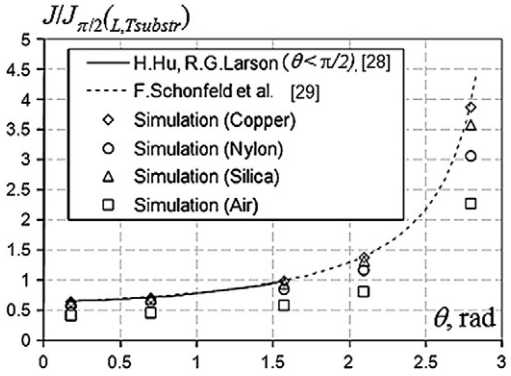

Fig. 5. Rescaled dependence of the total vapour flux from the droplet surface, J, on contact angle, θ, $L = 1$ mm. Both latent heat of vaporization and Marangoni convection were taken into account. Redrawn from [32].

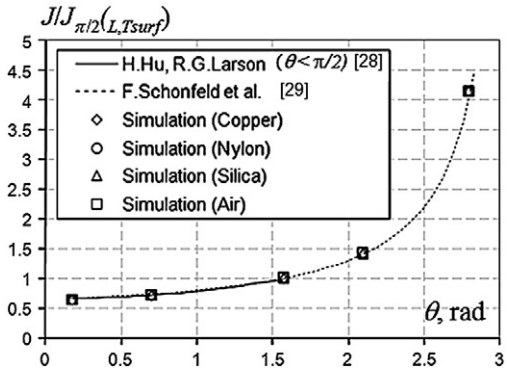

Fig. 6. Universal behaviour: rescaled dependence of the total vapour flux from the droplet surface, J, on contact angle, θ, $L = 1$ mm. Both LHV and MC are taken into account. All points from Fig. 5 are on the universal isothermal curve (the same as in Fig. 5) and indistinguishable, when T_{surf} used as the temperature of the droplet–air interface. Redrawn from [32].

In this case the vapour diffusion across the layer is controlled by the difference of vapour concentrations in the ambient air and at the droplet surface. The latter is a function of the local temperature at the surface. In the model under consideration [37] the surface of a droplet is cooled by the evaporation; meanwhile due to the high heat conductivity of the substrate the temperature of the contact line remains equal to the ambient one. As a result the higher temperature at the three phase contact line gives higher vapour concentration and more intensive evaporation flux at the droplet's perimeter (see Fig. 7).

4. Simultaneous spreading and evaporation in the case of complete wetting

In the case of complete wetting droplets spread out completely over a solid substrate, and contact angle decreases down to zero value. Lee et al. [40] considered the process of simultaneous spreading and evaporation of sessile droplets in the case of complete wetting. In order to model the spreading they considered Stokes equations under a low slope approximation [40]. The total evaporation flux, J, was used according to Eq. (1a). The whole process of spreading/evaporation was divided into two stages: (i) a first short but fast spreading stage, when the evaporation can be neglected, and the droplet volume, V, is approximately constant; and (ii) a second slower stage, when the spreading process is almost over, contact angle approximately constant, and evolution is determined mostly by the evaporation. On the basis of this analysis the droplet base radius, L, is considered as a function of the droplet volume, V, and contact angle, θ. Time derivative of $L(V,\theta)$ gives two velocities of the contact line:

$$\frac{dL(V,\theta)}{dt} = \frac{\partial L(V,\theta)}{\partial \theta}\frac{d\theta}{dt} + \frac{\partial L(V,\theta)}{\partial V}\frac{dV}{dt} = v_+ - v_-, \tag{6}$$

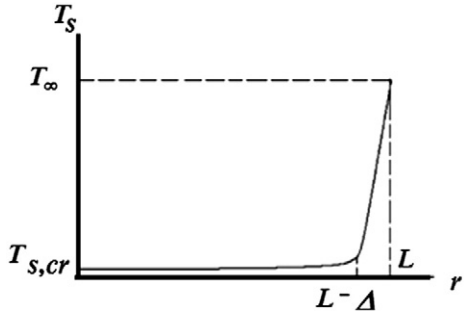

Fig. 7. Temperature distribution over the droplet surface, $T_s(r)$. r is the radial coordinate; $T_{s,cr}$ is the temperature of the droplet surface at which the evaporation flux vanishes; L is the radius of the droplet base; Δ is an area within the vicinity of the three-phase contact line, where evaporation mostly takes place. Redrawn from [39].

where v_+ is the spreading velocity, and v_- is the velocity due to the evaporation:

$$v_+ = \left.\frac{dL(V,\theta)}{dt}\right|_{V\approx const} = \frac{\partial L(V,\theta)}{\partial\theta}\frac{d\theta}{dt}, \tag{7}$$

$$v_- = -\left.\frac{dL(V,\theta)}{dt}\right|_{\theta\approx const} = -\frac{\partial L(V,\theta)}{\partial V}\frac{dV}{dt}. \tag{8}$$

The spreading velocity of the contact line, v_+, is obtained by Starov et al. in [41]:

$$v_+ = 0.1\left(\frac{4V}{\pi}\right)^{0.3}\left(\frac{10\gamma\omega}{\mu}\right)^{0.1}\frac{1}{(t+t_0)^{0.9}}, \tag{9}$$

where γ is the surface tension of the liquid; μ is the dynamic viscosity of the liquid; ω is the effective lubrication parameter [42]; and t_0 is the duration of the inertial stage of spreading when the capillary regime of spreading is not applicable [41]. Eq. (9) is derived from Eq. (7) using the expression for $L(t)$ obtained by Starov et al. in [42]:

$$L(t) = L_0\left(1+\frac{t}{\tau_0}\right)^{0.1}, \tag{10}$$

where L_0 is the droplet base radius after the very fast inertial stage is over and which is considered as an initial radius of the droplet base; $\tau_0 = \frac{3\mu L_0}{10\gamma}\left(\frac{\pi\lambda L_0^2}{4V}\right)^3$; λ is the dimensionless constant [41,42] connected to the effective lubrication parameter ω [41,42]. The velocity v_- is obtained from Eq. (8) using the Eq. (1b):

$$v_- = \frac{\alpha L^2}{3V}. \tag{11}$$

In the case of complete wetting the contact angles are small enough (less than 20°), and function $F(\theta)$ [27] varies from 0.64 to 0.68. That is, according to the previous discussion α can be considered as a constant with a good degree of approximation.

Substituting Eqs. (9) and (11) into Eq. (6) leads to the following equation:

$$\frac{dL}{dt} = 0.1\left(\frac{4V}{\pi}\right)^{0.3}\left(\frac{10\gamma\omega}{\mu}\right)^{0.1}\frac{1}{(t+t_0)^{0.9}} - \frac{\alpha L^2}{3V}. \tag{12}$$

The latter gives a system of two differential Eqs. (1b) (where α is a constant) and (12) with the following initial conditions [40]:

$$V(0) = V_0, \tag{13}$$

$$L(0) = L_0 = \left[\frac{10\gamma\omega}{\mu}\left(\frac{4V_0}{\pi}\right)^3\right]^{0.1} t_0^{0.1} \tag{14}$$

where V_0 is the initial droplet volume and L_0 is the droplet base radius after the very fast initial stage is over. Solution of this system of equations in non-dimensional form gives a universal law of process of simultaneous spreading and evaporation for the case of complete wetting, which is confirmed by experimental data from various literature sources [40] (see Figs. 8 and 9).

5. Simultaneous spreading and evaporation in the case of partial wetting

As we already mentioned above in the case of partial wetting contact angle hysteresis is the most important feature: in the presence of contact angle hysteresis the evaporation of a sessile droplet in nonsaturated vapour atmosphere goes through four consequent stages (Fig. 10).

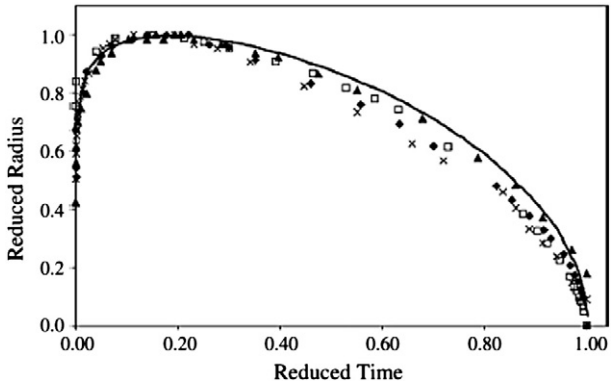

Fig. 8. Dependency of a reduced radius of the droplet base, L/L_0, against reduced time, t/τ_0, calculated according to Eqs. (1b) and (12) (solid line) for comparing different liquids spreading/evaporating on solid substrates. Experimental data extracted from various literature sources [40]:◆ — octane; □ — water; ▲ — silicon oil (3 μl); x — silicon oil (0.5 μl); solid line — theoretical prediction. Redrawn from [40].

Spreading stage. During this short stage immediately after a deposition both the contact angle and radius changes simultaneously reaching in the end values θ_{ad} and L_{ad}, correspondingly. These values are used as initial values for the following first stage. It is possible to neglect evaporation during spreading stage and, hence, it can be described using conventional hydrodynamic approach [1] (see also a consideration above on the static advancing contact angle). *Stage I* of evaporation. The contact angle decreases from θ_{ad} down to static receding contact angle, θ_r, at constant radius of the droplet base, $L = L_{ad}$. *Stage II* of evaporation. Contact angle remains constant and equal its receding value, θ_r, while the radius of the droplet base, L, decreases. *Stage III* of evaporation. Both the contact angle, θ, and the radius of the droplet base, L decrease until the drop disappears completely. This stage is also relatively shorter as compared with the stages one and two. Probably surface forces (disjoining/conjoining pressure) become important during this stage [1,11]. Some consideration of the third stage is undertaken below.

Below only two longest stages of evaporation, I and II, are under consideration.

Detailed study of stages I and II in the case of pure liquids has been performed in [43]. It was assumed in [43] that during both stages of evaporation the droplet retains the spherical shape. That is, the volume of the droplet, V, can be presented as follows:

$$V = L^3 f(\theta), \qquad f(\theta) = \frac{\pi}{3}\frac{(1-\cos\theta)^2(2+\cos\theta)}{\sin^3\theta}. \tag{15}$$

During both stages of evaporation, I and II, the mass conservation law has the form given by Eq. (1a), where the parameter β does not depend on the age of droplet as it was explained above and, hence, remains constant. There is a separate section in the end of this paper, where methods are presented for the calculation of parameter β.

5.1. The first stage of evaporation

During this stage of evaporation the radius of the contact line remains constant and equals to L_{ad} (Fig. 10). Hence, Eq. (1a) can be rewritten as $L_{ad}^3 f'(\theta)\frac{d\theta}{dt} = -\beta F(\theta) L_{ad}$,or:

$$L_{ad}^2 f'(\theta)\frac{d\theta}{dt} = -\beta F(\theta), \tag{16}$$

with the initial condition

$$\theta|_{t=t_{ad}} = \theta_{ad}. \tag{17}$$

Note, that the static advancing contact angle, θ_{ad}, should be taken from the experimental data, because it cannot be determined independently in

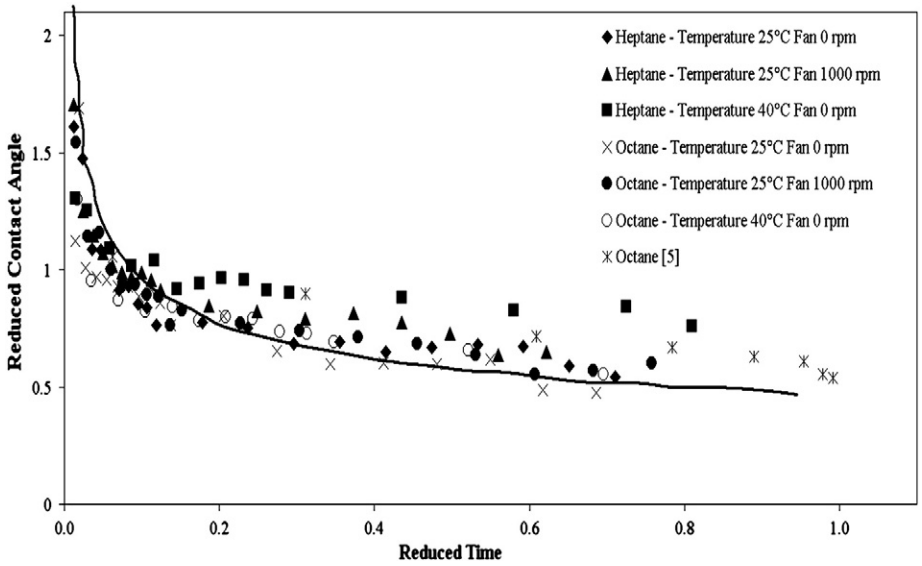

Fig. 9. A reduced contact angle θ/θ_m, where θ_m is a contact angle at the time when the droplet base radius reaches the max value, against a reduced time t/τ_0 calculated according to Eqs. (1b) and (12) (solid line) and experimental data from various sources. Redrawn from [40].

the framework of the theory presented. The following dimensionless time was introduced in [43]: $\tau = \frac{t-t_{ad}}{t_{ch}}$, where $t_{ch} = \frac{L_{ad}^2}{\beta}$ is the characteristic time of the process. Eq. (16) now takes the following form:

$$f^{'}(\theta)\frac{d\theta}{d\tau} = -F(\theta). \tag{18}$$

Direct integration of the latter equation with the boundary condition (17) results in

$$A(\theta, \theta_{ad}) = \tau, \tag{19}$$

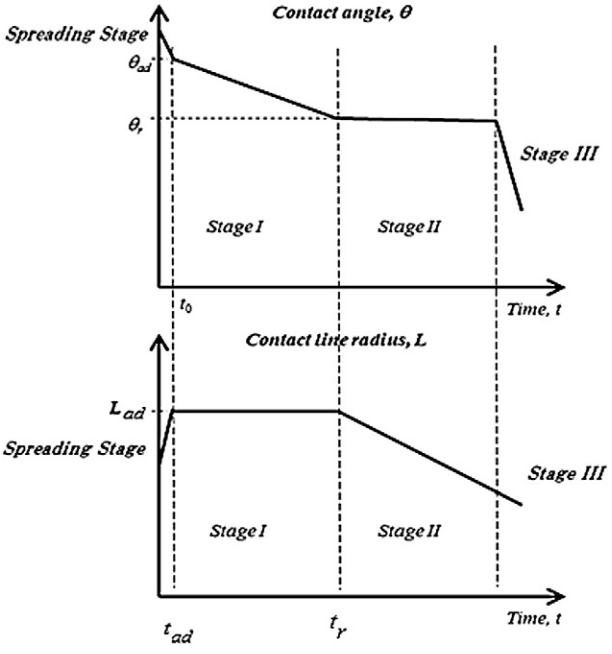

Fig. 10. Spreading stage and the three stages of evaporation in the case of partial wetting. Reprinted with permission from [47] Copyright (2013) American Chemical Society.

where $A(\theta, \theta_{ad}) = \int_{\theta}^{\theta_{ad}} \frac{f^{'}(\theta)}{F(\theta)} d\theta$. Eq. (19) shows that the deduced dependency should be universal and does not depend on the nature of the liquid and the droplet volume. The only parameter left is the initial contact angle (static advancing contact angle), which is supposed to be independently determined.

The first stage proceeds until the contact angle reaches its final value equal to the static receding contact angle. Using Eq. (19) we conclude that the end of the first stage, $\tau_r = \frac{t_r - t_{ad}}{t_{ch}}$, is determined as the moment when the contact angle reaches the value of a static receding contact angle, θ_r:

$$A(\theta_r, \theta_{ad}) = \tau_r, \tag{20}$$

where, again the static receding contact angle θ_r is supposed to be extracted from the experimental data.

Let us introduce a new dimensionless time. Eq. (19) can be rewritten as:

$$\int_{\theta}^{\pi/2} \frac{f^{'}(\theta)}{F(\theta)} d\theta = \tau + \int_{\theta_{ad}}^{\pi/2} \frac{f^{'}(\theta)}{F(\theta)} d\theta, \tag{21}$$

or

$$K(\theta) = \widetilde{\tau}, \tag{22}$$

where, $K(\theta) = \int_{\theta}^{\pi/2} \frac{f^{'}(\theta)}{F(\theta)} d\theta = A(\theta, \pi/2)$, and $\widetilde{\tau} = \tau + K(\theta_{ad})$ is a new dimensionless time. The contact angle π/2 was selected arbitrarily having in mind that comparison below will be undertaken mostly in the case of non-wetting.

Eq. (22) represents the unique curve describing the first stage of evaporation. Comparison of the presented theory with available experimental data from various literature sources is presented in Fig. 11 and shows a very good agreement between theory prediction and experimental data.

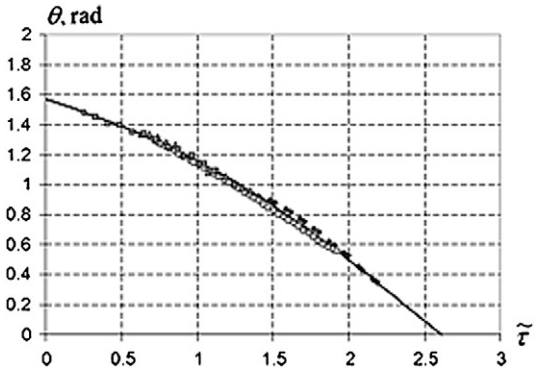

Fig. 11. Dependence of contact angle, θ, on dimensionless time, $\tilde{\tau}$ during the first stage of evaporation. Solid line is the theoretical prediction according to Eq. 22. Experimental points are taken from various literature sources. Redrawn from [43].

5.2. The second stage of evaporation

During this stage the contact angle remains constant but the radius of the contact line decreases. Hence, Eq. (1a) can be rewritten now as $3L^2 f(\theta_r)\frac{dL}{dt} = -\beta F(\theta_r)L$. Let us introduce the same dimensionless time, τ, as before and dimensionless radius of the contact line: $\ell = L/L_{ad}$. The latter equation can be rewritten as

$$\frac{d\ell^2}{d\tau} = -\frac{2}{3}\frac{F(\theta_r)}{f(\theta_r)}, \quad \tau > \tau_r \tag{23}$$

with the following initial condition: $\ell(\tau_r) = 1$. Direct integration of the Eq. (23) results in $\ell^2(\tau) = 1 - \frac{2F(\theta_r)}{3f(\theta_r)}(\tau - \tau_r)$, or:

$$\ell(\tau) = \sqrt{1 - \frac{2F(\theta_r)}{3f(\theta_r)}(\tau - \tau_r)}. \tag{24}$$

Eq. (24) gives a universal dependence during the second stage of evaporation.

Introduction of a new dimensionless time $\overline{\tau} = \frac{2F(\theta_r)}{3f(\theta_r)}(\tau - \tau_r)$ in the Eq. (24) results in the following universal dependency of the contact line on time:

$$\ell(\overline{\tau}) = \sqrt{1 - \overline{\tau}}. \tag{25}$$

Eq. (25) represents the unique curve describing the second stage of evaporation (Fig. 12).

Among other experimental evidences of the validity of proposed theory of diffusion-limited evaporation, Sobac and Brutin demonstrated it in their work [44]. They investigated the influence of the surface properties of substrates on the evaporation process. Various nanocoatings in their experiments allowed modifying the surface properties of substrates, such as the roughness and the surface energy, while maintaining constant thermal properties. Using five liquids and four coatings authors have got a wide range of experimental data with different dynamics of the triple line, different volatility of fluids, and a large range of values of wettability. Their experimental results are in very good quantitative agreement with existing models of quasi-steady, diffusion-driven evaporation. Authors confirm that the models succeed in describing the evaporative dynamics throughout the evaporation process regardless of the volatility of liquids and the behaviour of the triple line.

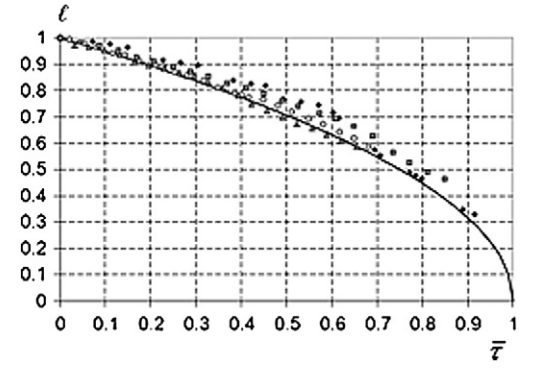

Fig. 12. Second stage of evaporation. Dependence of dimensionless radius of the contact line, ℓ, on dimensionless time, $\overline{\tau}$. Solid line is the theoretical prediction according to Eq. (25) Experimental points from various literature sources. Redrawn from [43].

6. Calculation of parameters in the case of complete and partial wetting

In the case of relatively big droplets, that are bigger than 1 μm, diffusive regime of evaporation prevails according to [45,46] and only such droplets were considered above and are considered below in this section.

The only parameter, which should be determined, is the parameter, β (see Eq. (1a)). Calculation of this parameter is very much different in the case of complete wetting and partial wetting.

6.1. Complete wetting case

In this case contact angle remains low from the beginning through the end of the spreading process: less than 20° in all experiments used in [40] for comparison of the theoretical predictions and experimental data. In this case the function $F(\theta)$ (Eq. (1a)) varies in between 0.64 and 0.68. That is in a good approximation can be considered as a constant. According to that function $F(\theta)$ was assumed a constant, that is, the parameter α in Eq. (1b) was considered as a constant to be determined. The parameter α in Eq. (1b) was calculated in the following way [40]. Eq. (1b) was integrated, which resulted in:

$$V = V_0 - \alpha\int_0^t L(t)dt. \tag{26}$$

Experimental dependencies of the volume of the droplet on time, $V(t)$, were plotted against $\int_0^t L(t)dt$. In all cases, $V(t)$ showed a linear trend (Fig. 13). Using these linear dependencies, the proportionality coefficient α was extracted [40].

6.2. Partial wetting

In this case the situation is completely different. Eq. (1a) is rewritten below in a different form to calculate the parameter β.

It is easily concluded that the droplet volume, V, can be expressed via the radius of the droplet base, L, and the contact angle, θ, according Eq. (15) as $L = \frac{V^{1/3}}{f^{1/3}(\theta)}$. Eq. (1a) can be rewritten now using the latter expression in the following form:

$$\frac{dV}{dt} = -\beta B(\theta)V^{1/3}, \quad B(\theta) = \frac{F(\theta)}{f^{1/3}(\theta)}. \tag{27}$$

In the case of partial wetting there are four stages of spreading/evaporation (see Fig. 10). As mentioned above only the longest stages I and II of evaporation are under consideration: stage I, when the radius of the droplet base remains constant, but the contact angle decreases over time from the initial value equal to static advancing contact angle, θ_{ad}, to static receding contact angle, θ_r; and the following stage II, when the contact angle remains constant and equal to the static receding contact angle, θ_r, while the radius of the droplet base shrinks.

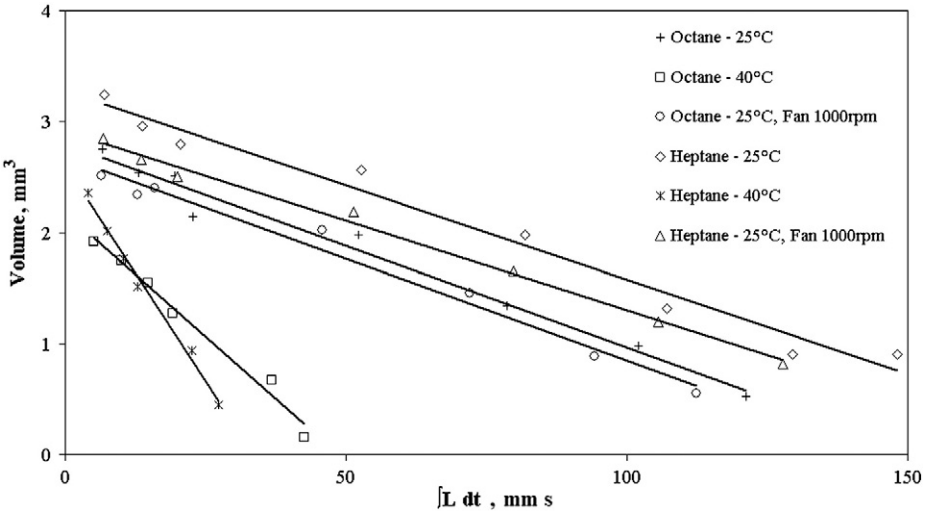

Fig. 13. Experimental dependences and straight lines fitted according to Eq. (26). Redrawn from [40].

The latter means that during the stage II function $B(\theta_r)$ remains constant.

In Fig. 14 the plot of function $B(\theta)$ is presented, showing that $B(\theta) \sim 0.8$ at $\theta > 40°$ and remains within a narrow limit between 1 and 0.8 when contact angle changes between 20° and 40°. The latter allows us to conclude that the function $B(\theta)$ can be considered a constant also during the stage I with a reasonable degree of approximation. Hence, we can rewrite Eq. (27) as

$$\frac{dV}{dt} = -\beta B(\theta_r) V^{1/3}, \quad V(0) = V_0. \tag{28}$$

Integration of the latter equation results in a well known dependency

$$V^{2/3}(t) = V_0^{2/3} - \frac{2\beta B(\theta_r)}{3} t. \tag{29}$$

Eq. (29) was well confirmed experimentally [47–49] and above we presented the proof why this dependency is really valid.

Below we show that the dependency (29) remains valid in the case of spreading/evaporation of both surfactant solutions and nanosuspensions.

Eq. (29) allows extracting the unknown parameter β using experimental data for $V(t)$. However, below we present a way of direct computer calculations of this parameter.

7. Evaporation of microdroplets of pure liquids

In all previous considerations only a diffusion model of evaporation was taken into account. However, according to Murisic and Kondic [50] this model is not always the right one. They considered theoretically, numerically and experimentally the evaporation of water and isopropanol drops on smooth silicon wafers, which proceeded without contact line pinning. Their theoretical model also includes Marangoni forces due to

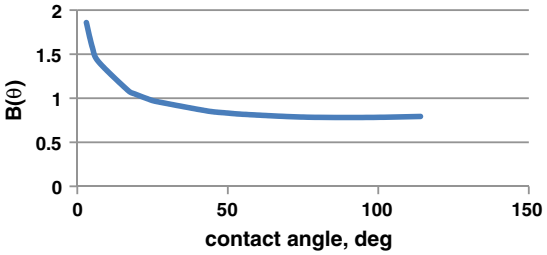

Fig. 14. Dependency of function $B(\theta)$ from Eq. (27) on contact angle.

the thermal gradients produced by non-uniform evaporation, and the heat conduction effects both in solid and liquid phases. They implemented two commonly used models of evaporation: vapour diffusion-limited evaporation and the evaporation limited by the processes in liquid. The authors of [50] have shown that two commonly used evaporation models lead to qualitatively different results, including drop evolution and thermal gradients along the liquid–gas interface. The procedure they used has effectively allowed for a direct comparison between the predictions of the two evaporation models corresponding to a particular physical set-up. Both models of droplet evaporation agreed with their experiments for different liquids.

The kinetic effects at the liquid–gas interface (Hertz–Knudsen–Langmuir equation), dependency of vapour pressure on the droplet curvature (Kelvin's equation), Stefan flow (the flow generated by the production of vapour phase) were neglected in the diffusion model of evaporation. It was shown in [45,46] that influence of these phenomena is negligible if the size of aqueous droplet is bigger than 1 μm. However, for smaller droplets these phenomena become important, and a smooth transition between diffusive and kinetic models of evaporation is observed for submicron drops of water.

By saying "kinetic effects" everywhere below we mean the effects which appear due to the fact that the rate of molecules transfer across the liquid–gas interface has a finite value. When this rate (represented by the well-known Hertz–Knudsen–Langmuir equation) is comparable to (or smaller than) the rate of vapour diffusion above the liquid–gas interface, then kinetic effects become noticeable or even dominate. Even though we take into account the finite rate of molecule transfer across the interface, we ignore the effect of vapour recoil, because the evaporation is not that intensive as evaporation into vacuum, and we believe that recoil pressure is negligible in our case.

Computer simulations of evaporation of small sessile droplets of water are performed in [45,46]. The adopted model [45,46] combines diffusive and mentioned above extra models of evaporation. The effect of latent heat of vaporization, thermal Marangoni convection and Stefan flow (generated by the production of vapour phase) in the surrounding gas was also taken into account. The investigated system was an aqueous droplet on a heat conductive substrate (copper) in air [45,46]. Results of modelling allowed estimating the characteristic droplet sizes when each of the mentioned above phenomena become important or can be neglected.

The model used in [45,46] is valid only for droplet size bigger than the radius of surface forces action, which is around 10^{-7} m = 0.1 μm. That is, the data presented in [45,46] for the droplet size smaller than 10^{-7} m are used only to show the trend. The results obtained in [45,46] can be summarised as follows: (i) deviation of the saturated

vapour pressure caused by the droplet curvature (Kelvin's equation) can be neglected when the radius of the droplet base, L, is bigger than 10^{-7} m, (ii) a deviation from the pure diffusion model of evaporation can be neglected for the droplet size bigger than 10^{-6} m, and (iii) deviations from diffusion model become noticeable only if the droplet size is less than 10^{-6} m. These deviations are caused by an increasing influence of the kinetic effects at the liquid–gas interface (Hertz–Knudsen–Langmuir equation) and this theory should be applied together with the diffusion equation of vapour in the air if the droplet size is less than 10^{-6} m.

The latter conclusions show that a consideration of evaporation of microdroplets with size that is less than 10^{-7} m should include both deviation of the saturated vapour pressure caused by the droplet curvature and the kinetic effects.

The latent heat of vaporization results in a temperature decrease at the surface of the droplet. Due to that, the evaporation rate is reduced. This effect is more pronounced in the case of diffusion limited evaporation ($L > 10^{-5}$ m), when vapour pressure at the droplet's surface is saturated and determined by local temperature. The effect of Marangoni convection in aqueous droplets is negligible for droplets of size $L < 10^{-5}$ m. For the system considered above, Stefan flow effect appeared to be weaker than the effect of thermal Marangoni convection for $L > 10^{-4}$ m, but stronger for $L < 10^{-4}$ m. However, in all cases its influence is small and can be neglected. The presented model [45,46] can be applied for evaporation of any other pure simple liquid not aqueous droplets only.

According to the model of diffusion limited evaporation the evaporation flux, $J_{c,i}$, must be linearly proportional to the droplet size, L, that is $J_{c,i} \sim L$. The latter is in agreement with the data presented in Fig. 15 for droplets bigger than 10^{-6} m. However, for a pure kinetic model of evaporation (no vapour diffusion, uniform vapour pressure in the gas) flux $J_{c,i}$ is supposed to be proportional to the area of the droplet's surface, that is in the case of pinned droplets (constant contact area) $J_{c,i} \sim L^2$ should be satisfied. To check the validity of the latter models at various droplet sizes it was assumed in [45,46] that the dependency of the evaporation flux on the droplet radius has the following form $J_{c,i} \sim A(\theta)\cdot L^n$, where n is the exponent to be extracted from computer simulation results [45,46] and A is a function of the contact angle, θ.

The calculated values of n are presented in Fig. 16. This figure shows that the exponent n, as expected, is equal to 1 for a pure diffusive isothermal model of evaporation within the whole studied range of L values (diamonds in Fig. 16). Fig. 16 shows that that the diffusion model of evaporation dominates for droplets with the size bigger than 10^{-5} m, that is for droplets bigger than 10 μm even in the case when both kinetics effects and Kelvin's equation are taken into account additional to the pure diffusion.

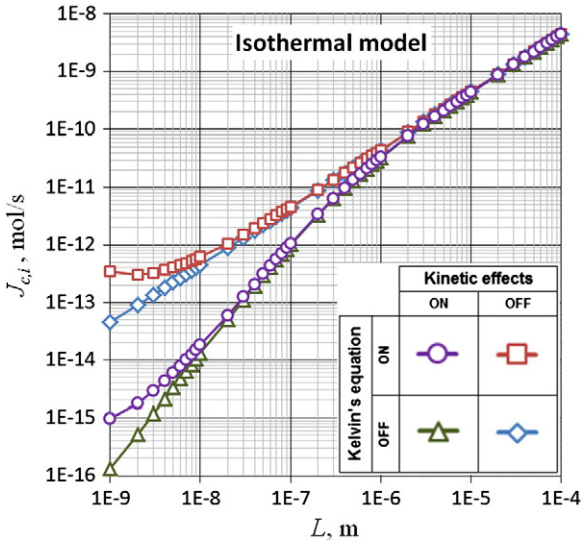

Fig. 15. Dependence of the aqueous droplet's total molar evaporation flux, $J_{c,i}$, on the droplet size, L, for isothermal model of evaporation. Parameters used: $\theta = 90°$; relative air humidity is 70%. Note: results for $L < 10^{-7}$ m do not have physical meaning, as additional surface forces must be included into the model. These points are shown to demonstrate the trends of curves. Reprinted with permission from [46] Copyright (2012) American Chemical Society.

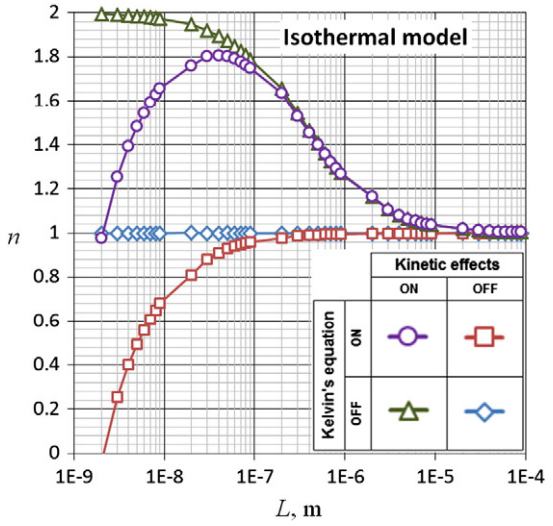

Fig. 16. Exponent n for the dependence $J_{c,i} \sim A(\theta)\cdot L^n$ for the isothermal model of evaporation. Parameters used: $\theta = 90°$; relative air humidity is 70%. Note: results for $L < 10^{-7}$ m do not have physical meaning, as surface forces action must be included into the model here. These points are shown to demonstrate the trends of curves. Reprinted with permission from [46] Copyright (2012) American Chemical Society.

Taking into account kinetic effects only additional to the diffusion without Kelvin's equation (triangles in Fig. 16) results in a smooth transition from the linear dependence $J_{c,i} \sim L$, that is $n = 1$ (diffusive model) to the quadratic one $J_{c,i} \sim L^2$, that is $n = 2$ (kinetic model) as the size of the droplet decreases down to $L = 10^{-9}$ m (see Fig. 16). The latter shows that $J_{c,i}$ tends to be proportional to L^2 as the size of the droplet decreases, which means that evaporation flux becomes proportional to the area of the liquid–gas interface. However, the influence of the curvature (Kelvin's equation) on the saturated vapour pressure results in a substantially lower exponent n as compared with the kinetic theory (Fig. 16). Note that the latter happens only for a droplet completely in the range of surface forces action, that is, less than 10^{-7} m [1]. Below this limit the droplet does not have a spherical cap shape any more even on the droplet's top (microdroplets according to Ref. [1]). Evaporation process in the latter case should be substantially different from the considered above. Thus the range of sizes less than 10^{-7} m is not covered by the presented theory.

8. Evaporation kinetics of nanosuspensions of inorganic particles

Evaporation kinetics of relatively big (bigger than 1 μm) sessile droplets of aqueous suspension of inorganic nanoparticles on solid substrates of various wettability is investigated from both experimental and theoretical points of view in [49]. The following nanoparticles were used: silicon dioxide (labelled below as SiO_2), titanium dioxide (labelled below as TiO_2) and carbon nanopowder (C). Two types of carbon nanoparticles have been used: carbon nanoparticles with size <50 nm (labelled below as C50) and carbon nanoparticles with size <500 nm (labelled below as C500). The SiO_2 and TiO_2 particles had an average diameter of 10–20 nm and approximately 21 nm, respectively. Carbon nanoparticles were subjected to the annealing procedure in Dr. Mattia's laboratory at the University of Bath, UK according to the procedure presented in [51]. The volume fraction of particles was 1% for all suspensions studied. Three kinds of solid substrates of different wetting properties and different thermal conductivities were used: smooth silicon wafers, ultra high molecular weight polyethylene films (PE) and polytetrafluoroethylene films (referred to as PTFE). Experimental results on the evaporation of

Table 1
Static advancing, θ_{ad}, and static receding, θ_r, contact angles, $B(\theta_{ad})$, $B(\theta_r)$ and number of stages for aqueous nanosuspensions on (a) PE, (b) silicon wafer and (c) PTFE substrates.

	θ_{ad}	θ_r	$B(\theta_{ad})$	$B(\theta_r)$	Number of stages
a) PE					
H_2O	98	74	0.78	0.78	2
SiO_2	97	81	0.78	0.78	2
TiO_2	93	<49	0.78	0.83	1
C50	96	75	0.78	0.78	2
C500	93	<43	0.78	0.85	1
b) Si wafers					
H_2O	55	<26	0.81	0.96	1
SiO_2	42	<24	0.86	0.98	1
TiO_2	33	<19	0.90	1.05	1
C50	50	<17	0.83	1.08	1
C500	50	<24	0.83	0.98	1
c) PTFE					
H_2O	111	93	0.79	0.78	2
SiO_2	114	93	0.79	0.78	2
TiO_2	114	<75	0.79	0.79	1
C50	112	97	0.79	0.78	2
C500	113	<70	0.79	0.79	1

various kinds of inorganic nanosuspensions on solid surfaces of different hydrophobicity/hydrophilicity are compared with the theoretical predictions of diffusion limited evaporation of sessile droplets of pure liquids in the presence of contact angle hysteresis discussed above and a very good agreement is found for both evaporation stages.

Note that static advancing, θ_{ad}, and static receding, θ_r, contact angles cannot be determined independently from the theory used below. That is, these contact angles were taken from experimental results [49]. It is shown in [49] that the kinetics of evaporation of the above mentioned aqueous nanosuspensions is in a good agreement with the theory developed for pure liquids. The differences from the pure liquids are (i) static advancing and receding contact angles, which are different for each nanosuspension used and they differ from the corresponding values for the pure water and (ii) value of the parameter β.

In some cases two stages of evaporation were observed (stages I and II), while in other cases only stage I was detected [49].

Table 1 presents the values of static advancing, θ_{ad}, and static receding, θ_r, contact angles in degrees and calculated values of $B(\theta_{ad})$ and $B(\theta_r)$ (see Eq. (27)) for the nanosuspensions studied. In Table 1 the value of receding contact angle in the case of experiments where only one stage was observed is the last one measured before the droplet disappears or it was no longer of the spherical cap shape. In these cases droplet size was too small to continue the measurements.

According to Table 1 all values of $B(\theta)$ are in the range of 0.78 to 1.08 for contact angles ranging from 40 to 120°. This means that $B(\theta)$ can be considered as a constant with a reasonable degree of approximation when the contact angle ranges between θ_{ad} and θ_r and is independent of both the nanoparticle and the substrate nature.

Table 1 shows that the dependency (29) for volume on time should be valid. Experimental results in [49] confirm this assumption: dependency of volume on time really coincides with that predicted by Eq. (29). The latter allowed to extract parameter β from the slope of these dependences [49].

In Fig. 17 the experimental data on the first stage of evaporation are summarised for all the nanosuspensions studied in [49]. The solid line in Fig. 17 represents the theoretical prediction according to Eq. (22). Comparison shows a good agreement between the theoretical curve predicted by the theory for pure water and the experimental data. Notice that the negative values of the dimensionless time for this stage are due to the fact that $\tilde{\tau} = 0$ was arbitrarily selected as $\theta = \pi/2$, thus negative values correspond to $\theta > \pi/2$. Fig. 18 presents a summary of data for the second stage of evaporation for all nanosuspensions investigated on all solid substrates used, where the evaporation process showed this stage (see Table 1). Figs. 17 and 18 display that there is a good agreement between the theoretical predictions for both stages of evaporation (developed for pure liquids) and experimental data on evaporation (in the range of experimental error $\pm 10\%$).

8.1. Pattern formation on the solid

After evaporation process of nanosuspensions is finished different patterns are observed on solid surfaces. Pattern formation after evaporation of suspensions was reviewed in [52]. Below we add only few interesting phenomena observed in the case under consideration [49].

According to Table 1 [49] all pairs nanosuspensions of inorganic particles/substrates investigated can be subdivided into two groups: (i) those which evaporated during first stage only and (ii) those which evaporated in two stages. Particles accumulated at the centre of spot like in the case of carbon nanoparticles C50 nm on PE (Fig. 19a and b), in the case of two stages of evaporation, or at the edges like TiO_2 on PE (Fig. 19c) and in the case when only one stage of evaporation was

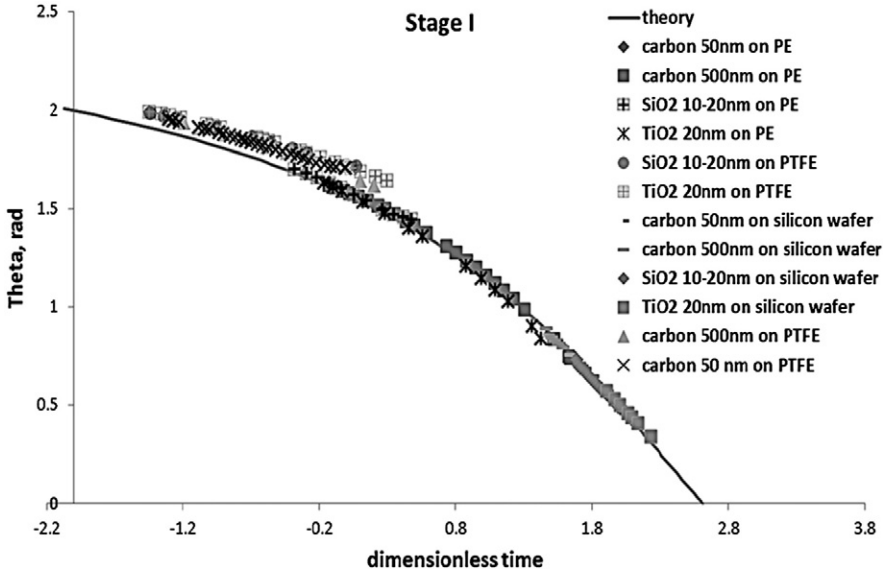

Fig. 17. First stage of evaporation. Summary of all nanosuspensions investigated on all solid substrates used in [48]. Redrown from [49].

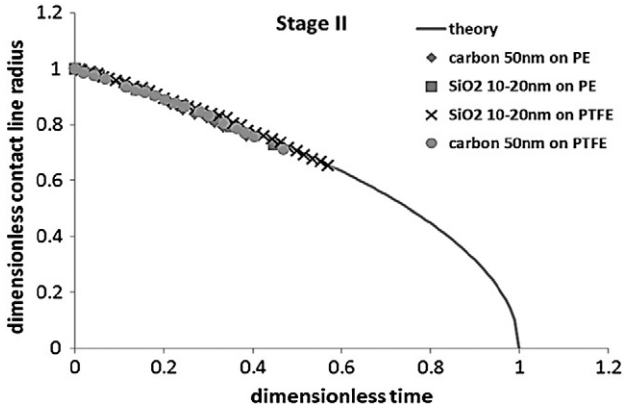

Fig. 18. Second stage of evaporation. Summary of all nanosuspensions investigated on all solid substrates used in [48], where the evaporation process showed the second stage of evaporation (see Table 1). Redrawn from [49].

detected. In the case (i) no traceable amount of particles was detected behind the receding three phase contact line.

Theoretical explanation of the observed pattern requires further investigations. For example, Popov [53] considered the deposit patterns in evaporating sessile drops of a colloidal solution on a plane substrate. His model is based on the assumption that the solute particles occupy the finite volume and hence the deposit dimensions are of a steric origin. Within the model, proposed by Popov, the geometrical characteristics of the deposition patterns are found as functions of the initial concentration of the solute, the initial geometry of the drop, and the time elapsed from the beginning of the drying process. The model was solved analytically for small initial concentrations of the solute and numerically for arbitrary initial concentrations of the solute. The results are validated against experimental data, and it is shown that the observed dependence of the deposit dimensions on the experimental parameters can indeed be attributed to the finite dimensions of the solute particles. These results are important for understanding the evaporative deposition.

9. Wetting and evaporation of droplets of surfactant solutions

The previously developed theory for evaporation of droplets of pure liquid was applied for investigation of kinetics of evaporation of surfactant solutions. In this case relatively big droplets are under consideration, that is a diffusion kinetics of evaporation can be applied.

Kinetics of evaporation of droplets of aqueous solutions of SILWET L77 on highly hydrophobic substrate was investigated in [48]. This surfactant was chosen because it is a superspreader [54–57], i.e. aqueous solutions of SILWET L77 demonstrate complete wetting on moderately hydrophobic substrates. A pH 7.0 buffer was used in this study as a solvent to prevent hydrolysis of the SILWET L77. Silicon wafers covered by amorphous Teflon (TEFLON-AF below) were used as hydrophobic substrates. The macroscopic contact angle of either pure water or buffer solution was ($118 \pm 2°$) on those substrates. Drops of 4 mm^3 were deposited onto the substrate for measurements. Five independent measurements were performed for each experimental point reported and the average was used. The experimental technique used was similar to the one used earlier by Ivanova et al. [58,59].

The spreading and evaporation of droplets of surfactant solutions demonstrate four stages as in the case of pure liquids (Fig. 10). As discussed in detail by Svitova et al. [60] and Ivanova et al. [59], during the spreading process (initial stage) it is possible to use a power-law dependency of the contact angle on time. In experiments presented in [48] the characteristic time scale of the initial stage of spreading was found to be in the range of t_{ad}–50 *s*. This value is similar to those found in Ref. [59] for aqueous trisiloxane solutions. This stage is short enough, less than 100 s, and the volume change is less than 5% [59] and, hence, it is possible to neglect evaporation during this stage.

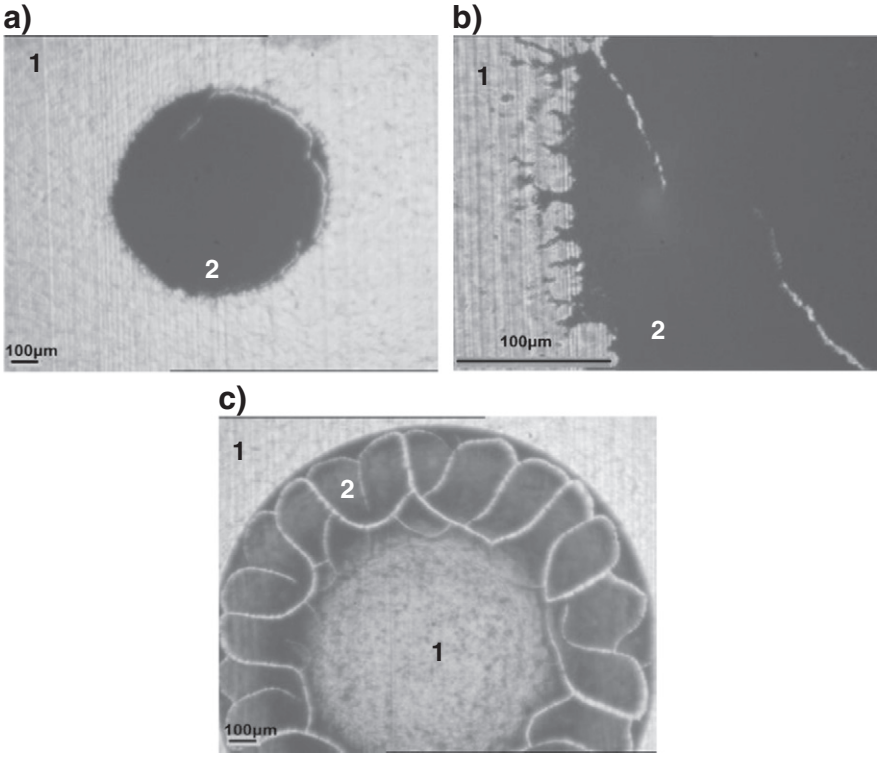

Fig. 19. Microscope pictures of patterns formed after evaporation of nanosuspensions (a) C50 nm on PE — whole spot, (b) — magnification of the edge (two stages of evaporation), and (c) TiO_2 on PE (only one first stage of evaporation); 1 — bare surface, 2 — deposit. Redrawn from [48].

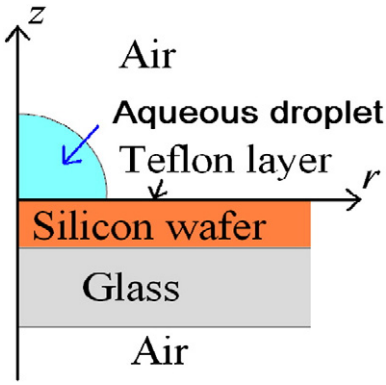

Fig. 20. Sketch of the solid support adopted for calculations of parameter β. An aqueous droplet is placed on silicon wafer, covered with a thin amorphous Teflon layer. The silicon wafer is placed on a thick glass support. Reprinted with permission from [47] Copyright (2013) American Chemical Society.

9.1. Calculation of parameter β

The previous consideration shows that β is the only parameter in the above theory (see Eq. (1a)). Above we described a procedure of extracting this parameter from experimental data in the case of complete wetting (Eq. (26)) and partial wetting (Eq. (29)). However, there is a possibility to calculate the parameter β using a more sophisticated method presented in [32] based on the direct computer simulations of the evaporation process. This procedure is presented below.

The schematic presentation of the solid support used for the measurements of the evaporation of aqueous surfactant solutions is shown in Fig. 20 and the computational scheme was developed accordingly.

The geometrical and physical parameters, which were selected for calculations are shown in [48].

Parameter β was extracted from the results of computer simulations as $\beta = \frac{J}{\rho_l F(\theta) L}$, where J is the total mass flux of droplet evaporation, ρ_l is water density, L is the radius of the droplet base, and $F(\theta)$ is the function of contact angle determined by Picknett and Bexon [27]. Numerical modelling described in [32] was used to predict the dependence of β on the ambient temperature, T_∞ and humidity H.

Figs. 21 and 22 show that the parameter β decreases with the increasing of relative humidity, H, at constant ambient temperature, T_∞, and increases with temperature at constant humidity. The experimental results confirm the trends shown by the computer calculations (Figs. 21 and 22): a) for a given temperature, T, the parameter β decreases as H increases; and b) for a given humidity, H, the parameter β increases with T.

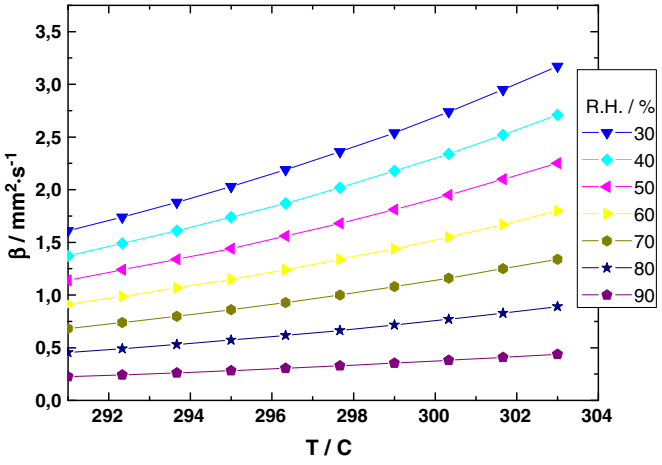

Fig. 21. Calculated parameter β as a function of temperature of the ambient air at various relative humidities. Reprinted with permission from [47] Copyright (2013) American Chemical Society.

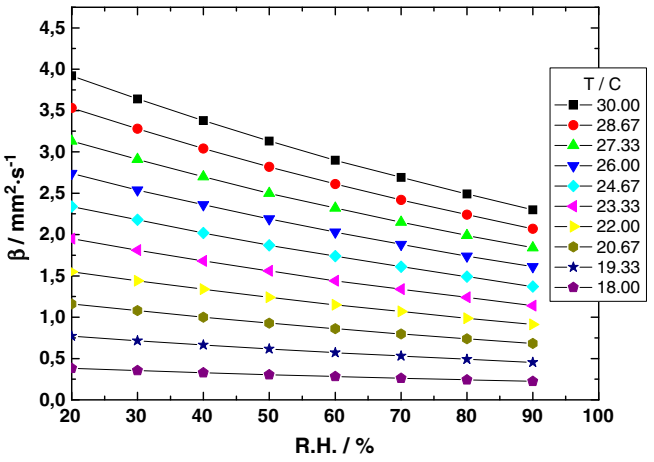

Fig. 22. Calculated parameter β as a function of a humidity of the ambient air at various temperatures. Reprinted with permission from [47] Copyright (2013) American Chemical Society.

In all experiments presented in [47,48] (see below) similarly to experiments with pure liquids and nanofluids discussed above a linear dependence $V^{2/3}(t) = V_0^{2/3} - const \cdot t$ was found, where $V(t)$ is the dependence of the volume of evaporating droplet on time (see Eq. (29)).

Introducing dimensionless time $\tau = \frac{\beta t}{V_0^{2/3}}$ we can rewrite Eq. (29) as

$$\left(\frac{V(t)}{V_0}\right)^{2/3} = 1 - \frac{2B}{3}\tau. \tag{30}$$

All experimental dependences of volume on time obtained for all concentrations studied in [48] agree with the linear dependence given by Eq. (30) (see Fig. 23). Note, that concentrations in Fig. 23 are normalized by critical aggregation concentration (critical aggregation concentration, CAC, is the concentration at which aggregates, for example micelles, spontaneously appear in the bulk solution; for SILWET L77 CAC = 0.1 g/l [61]).

According to [48] all receding and advancing contact angles for solutions studied were inside the range from 43° to 115°. Calculations according to Eq. (27) show that in this range of contact angles $B(\theta)$ varies from 0.79 to 0.86.

Fig. 23 shows an excellent linear fit, which gives $\frac{2}{3}B = 0.5649$ and, hence, $B = 0.84735$, that is, inside the mentioned above range (from 0.79 to 0.86). All other experimental dependences of volume on time follow the linear trend predicted by Eq. (30) [48].

Important to note that experimental values of both advancing and receding contact angles are used. Those values cannot be predicted in the framework of the above theory.

Fig. 10 shows a qualitative behaviour of contact angle, θ, and the radius of the droplet base, L, for pure aqueous droplets. Similar behaviour

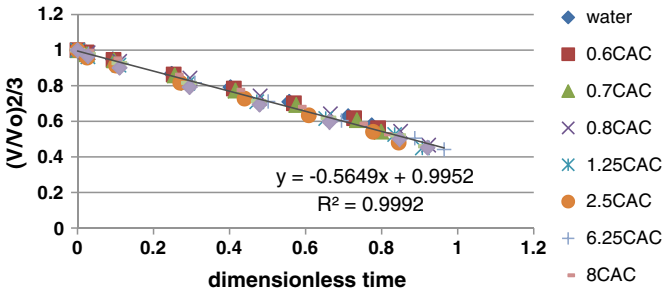

Fig. 23. An experimental dependency of reduced volume of evaporating droplet on reduced time (Eq. (30)) for different SILWET L77 concentrations at ambient temperature 24 °C and relative humidity 50%. The value of β is taken from Figs. 21 and 22. Reprinted with permission from [47] Copyright (2013) American Chemical Society.

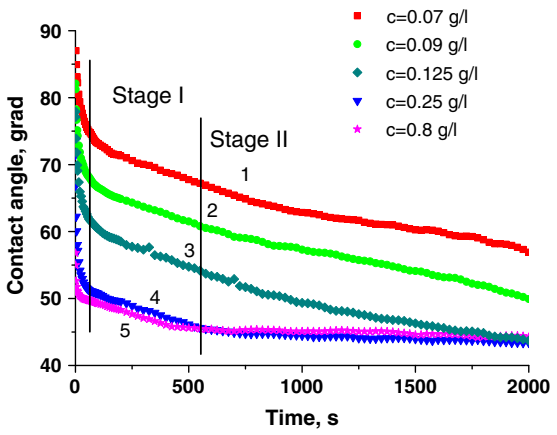

Fig. 24. Time dependence of the contact angle for different concentrations of SILWET L77 at temperature 24 °C and relative humidity 50%: 1 — C = 0.07 g/l, 2 — C = 0.09 g/l, 3 — C = 0.125 g/l, 4 — C = 0.25 g/l (CWC), and 5 — C = 0.8 g/l. The final third stage is not shown. Adapted with permission from [48] Copyright (2013) American Chemical Society.

was observed [48] for aqueous SILWET L77 solution at concentration above critical wetting concentration (critical wetting concentration, CWC, is the concentration of surfactant above which surfactant solution spreads completely on moderately hydrophobic substrates or its contact angle does not change any more on more hydrophobic substrates; as a rule CWC is several times higher than CAC; for SILWET L77 CWC = 0.40 mmol/l = 0.25 g/l = 2.5CAC [62]).

The time dependence of the radius of the droplet base for all solutions studied in [48], independently of concentration is similar to that presented schematically in Fig. 10 with L_{ad} increasing as the surfactant concentration increases.

Fig. 24 shows time dependences of contact angle, θ, for the SILWET L77 aqueous solutions over the investigated concentration range. As expected, the increase of surfactant concentration reduces both the initial contact angle (at the beginning of the spreading stage at the moment $t = 0$) and the static advancing contact angle (in the end of the spreading stage). It is important to note that according to Fig. 24 the static receding contact angle, θ_r, does not remain constant during the second stage, but varies with time at concentrations below CWC (curves 1–3 in Fig. 24), however it does not vary any more if surfactant concentration is above CWC (curves 4, 5 in Fig. 24).

Fig. 25 shows the dependence of static advancing, θ_{ad}, and static receding, θ_r, contact angles on initial surfactant concentration, C, for aqueous solutions of surfactant SILWET L-77. Values of both contact angles are presented in Fig. 25 obtained from the experimental data presented in Fig. 24 and similar data for other concentrations in the following way: static advancing contact angle, θ_{ad}, is equal to the contact angle at the end of spreading process (beginning of stage I in Fig. 24); static receding contact angle is equal to the contact angle at the end of stage one, that is, at the moment when the radius of the droplet base starts to decrease. Note, the lines depicting the stages in Fig. 24 are only schematic ones and the actual beginning of stage I and stage II for each curve in Fig. 24 can deviate slightly from the points of their intersection with the lines.

It looks like that not only advancing but also receding contact angles level off above CWC (for SILWET L-77 CWC = 0.25 g/l [62]) Dependency of the static advancing contact angle on concentration presented in Fig. 23 is in good agreement with the previous investigation [62].

The statistic advancing contact angle presented in Fig. 25 was determined at the beginning of stage one, when the surfactant concentration was almost identical to the initial concentration. However, the static receding contact angle was determined in the end of the first stage, when the surfactant concentration could be considerably higher as compared with the initial concentration because of evaporation. Note that in the case of concentrations below CWC the receding contact angle continued to decrease over the whole duration of the second stage of evaporation process. That is, the actual concentration is different from the initial one.

9.2. Comparison of the experimental data for evaporation of surfactant solutions with the theoretical predictions for pure liquids

Below the theoretical predictions for pure water are compared with the experimental results for aqueous surfactant solutions. Note again that both advancing and receding contact angles and their dependences on surfactant concentrations were extracted from the experimental data. These angles presented in Fig. 25 are very much different from those for water. Nevertheless, according to [48] the kinetics of evaporation of surfactant solutions is very similar to that of pure aqueous droplets. The main differences in the case of surfactant solutions are (i) the lower values of initial contact angles and as a consequence (ii) larger initial radiuses of the droplet base at all concentrations; and (iii) dependency of the receding contact angle on time during the second stage at concentrations below CWC.

Fig. 23 confirms that all slopes of $V^{2/3}(t)$ linear dependences are equal to that of pure aqueous droplet within experimental error. According to Eq. (30) these slops are proportional to the parameter β. Fig. 23 and Eq. (30) confirm that the parameter β does not depend on the concentration of surfactants and, hence, the rate of evaporation does not according to Eq. (1a).

It was found in [48] that the experimental data follow the predicted universal curve during the first stage of evaporation for all investigated temperatures, relative humidities and concentrations (72 sets of θ, V and L vs. t data).

However, the situation is more complex for the second stage of the spreading/evaporation, though the agreement with the theoretical predictions is still rather good. Fig. 26 shows as an example the data for concentrations below and above CAC obtained at temperature 30 °C and relative humidity 30%. According to [48] all other investigated cases show the same behaviour.

It is seen from Fig. 26 that there is a very good agreement with the theoretical predictions at concentrations above CWC and there are deviations from the theoretical predictions at concentrations below CWC. This may be understood considering that for the 0 < C < CAC < CWC the air/liquid and solid/liquid interfacial tensions change as the evaporation progresses due to the increase of concentration. The receding contact angle decreases as concentration increases in the range C < CWC. The latter phenomenon was not included in either the computer simulations or the theory above. This may also explain why the agreement between theory and experiment for pure water is similar to that of the more concentrated surfactant solutions at concentrations above CWC.

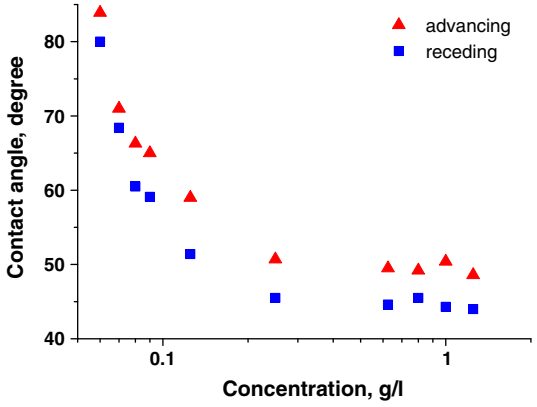

Fig. 25. Experimental dependence of advancing and receding contact angles on initial surfactant concentration for aqueous solutions of SILWET L-77. Reprinted with permission from [47] Copyright (2013) American Chemical Society.

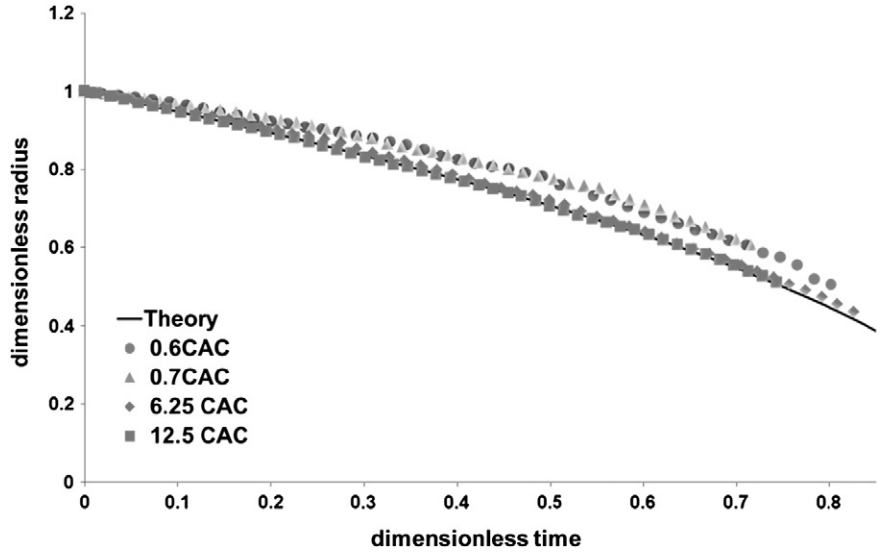

Fig. 26. Comparison of the experimental results for SILWET L77 aqueous solutions for the second stage of evaporation with the universal curve predicted by the theory for pure liquids (Eq. (25)). Example for relative humidity 30% and temperature 30 °C. Note once more, to plot the dependences presented in Fig. 26 experimental values of advancing and receding contact angles were used. Reprinted with permission from [48] Copyright (2013) American Chemical Society.

In Fig. 27 the experimental data published by Doganci et al. [47] for their experiments using SDS surfactant (55% RH, 21 °C) together with the results for SILWET L-77 (90% RH, 18 °C) [48] are presented. Fig. 27 proves that the agreement with theoretical predictions is similar for both surfactants although the scattering around the universal curve for the second evaporation stage seems to be higher for the SDS data.

There are two different processes causing the change in the surfactant bulk concentration during spreading/evaporation: (i) the concentration decreases due to depletion caused by the adsorption and (ii) increases because of the decrease of volume due to evaporation. Estimations made in [48] have shown that for droplet size used the initial bulk concentration equal to CAC should decrease on about 10% due to adsorption on both liquid/air and liquid/solid interface and about 35% should be adsorbed at the initial bulk concentration of 0.1 CAC. The latter means that the adsorption will result in a substantial decrease of the bulk concentration inside the droplet and as a result in a significant change of both advancing and receding contact angles. Evaporation results in an increase of surfactant concentration and simultaneously its redistribution between the bulk and interfaces due to the decrease of droplet volume affecting further the value of receding contact angle. All those processes have to be taken into account to improve the theory describing spreading/evaporation of surfactant solutions.

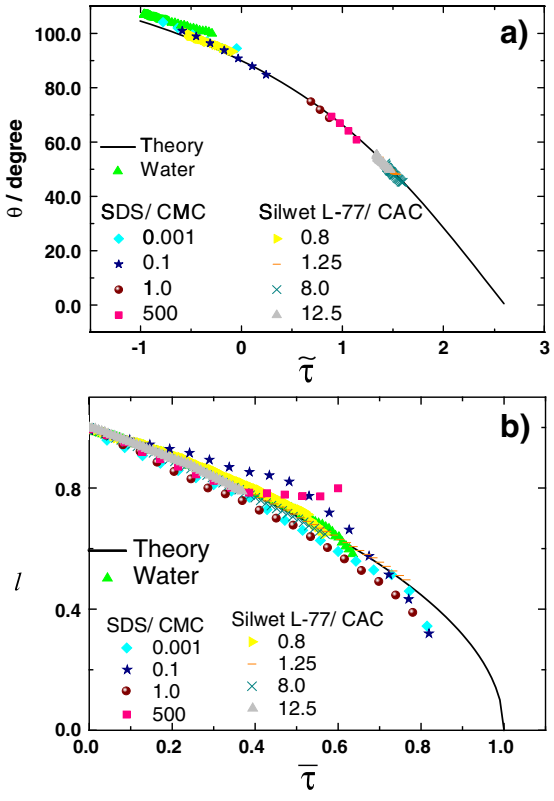

Fig. 27. Comparison of the universal behaviour predicted by the theory for pure liquids and experimental results of SDS [47] and of SILWET L77 [48] solutions for (a) first stage of evaporation and (b) second stage of evaporation. Reprinted with permission from [47] Copyright (2013) American Chemical Society.

9.3. The third stage of evaporation

The results presented in [48] show (Fig. 28) that the third stage of evaporation is much shorter than the first and second stages. The initial spreading stage is too short and is not shown in Fig. 28. The contact angle deviates from the static receding contact angle, θ_r, and decreases relatively fast during the third stage (Fig. 28). The latter is the problem for a theoretical description of the process during this stage. It is well-known that the receding contact angle can decrease at relatively high receding velocity, however estimations performed in [48] show that this is not the case.

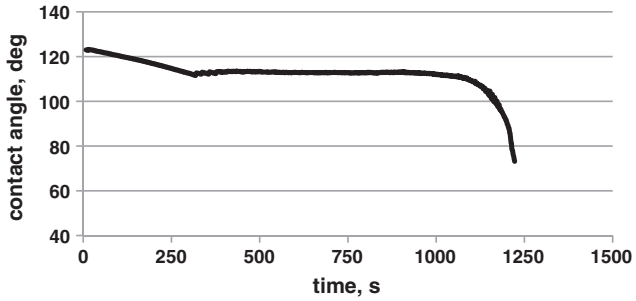

Fig. 28. A single experiment on evaporation of a pure water droplet at 24 °C at 50% humidity on Teflon covered silicon wafer. Reprinted with permission from [47] Copyright (2013) American Chemical Society.

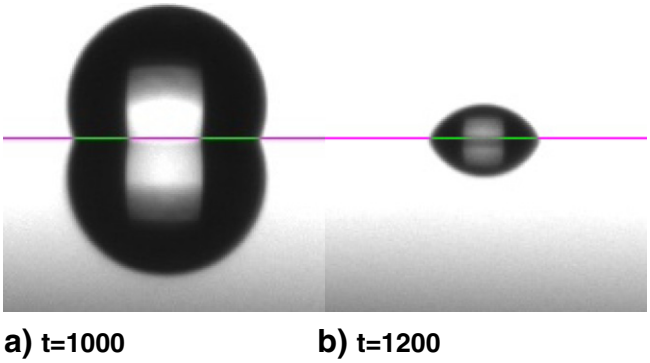

Fig. 29. Snapshot of evaporating droplet at two consecutive moments close to the moment when a sharp decrease of the contact angle takes place (Fig. 28). Reprinted with permission from [47] Copyright (2013) American Chemical Society.

Fig. 29 shows that during the third stage a sharp transition from $\theta_r > 90°$ (non-wetting) to $\theta_r < 90°$ (partial wetting) takes place. It is well established that both static advancing and static receding contact angles on smooth homogeneous substrates (like we used in our experiments) are completely determined by surface forces action in a vicinity of the three phase contact line [1,2]. These forces are well known in the case of partial wetting (modified DLVO theory), but very little is known in the case of non-wetting. Therefore, it has been assumed in [48] that in the case of non-wetting those forces are considerably different from the case of partial wetting and that just this transition from non-wetting to partial wetting is responsible for the occurrence of the third stage.

10. Conclusions

The considerable progress has been achieved during the last decade in understanding spreading and evaporation of liquid droplets on various solid substrates. It has been shown that interactions in vicinity of three-phase contact line and, in particular, disjoining pressure in this region are crucial for the processes under consideration. For example, the nature of hysteresis of the contact angle has been explained via the s-shape of isotherm of Derjaguin's pressure in the case of partial wetting. In this case hysteresis of the contact angle can be observed even of molecularly smooth substrates.

Kinetics of a simultaneous spreading/evaporation was described theoretically for the cases of complete and partial wetting of pure liquids. In the case of complete wetting the spreading/evaporation process proceeds in two stages. A theory was suggested for this case and a good agreement with available experimental data was achieved. In the case of partial wetting the evaporation of a sessile droplet in nonsaturated vapour atmosphere goes through four consequent stages: (i) — initial stage, spreading, is very short (1–2 min) and therefore evaporation can be neglected during this stage; during the initial stage contact angle reaches the value of advancing contact angle and the radius of droplet base reaches its maximum, (ii) — the first stage of evaporation is characterised by a constant value of the radius of the droplet base; the value of the contact angle during the first stage decreases from advancing to receding contact angle; (iii) — during the second stage of evaporation the contact angle remains constant and equal to its receding value, while the radius of the droplet base decreases; and (iv) — at the third stage of evaporation both the contact angle and the radius of the droplet base decrease until the drop completely disappears; this stage is also relatively short compared with the stages one and two of evaporation.

It has been shown theoretically and confirmed experimentally that during the stages I and II of evaporation the volume of the droplet to power 2/3 decreases linearly with time. If dimensionless variables are used then the time dependence of the contact angle during the first stage and of the radius of the droplet base during the second stage are represented by a universal curve, independent of the liquid and substrate used.

The kinetic effects at liquid–gas interface (Hertz–Knudsen–Langmuir equation), the dependence of vapour pressure on the droplet curvature, and the Stefan flow should be taken into considerations for the case of nanodroplets. Influence of these phenomena is negligible if the size of aqueous droplet is bigger than 1 μm.

The theoretical predictions made for pure liquids have been applied to analyse experimental results obtained for nanofluids (suspensions containing nano-particles) and surfactant solutions. It turned out that the theory developed for pure liquids is applicable for these systems as well. The deviations from the theoretical predictions have been found in description of the second stage of evaporations for surfactants at concentrations below critical aggregation concentration, because in this case the surfactant concentration and, therefore, the contact angle have been changing during the second stage because of the decrease of the volume. Nevertheless even in this case the agreement between the experimental data and the theory developed for pure liquids is rather good.

For certain combinations of particles/substrate the only first stage of evaporation was observed for nanofluids. Spreading/evaporation of nanofluids results in pattern formation with topology depending on particles and solid substrates used.

The theoretical description of the final stage of evaporation is to be developed. Most probably the surface forces play a considerable role at this stage and have to be taken into account.

Acknowledgements

This work was supported in part by the MICINN under grant FIS2012-28231-C02-01, by ESA under grants FASES and PASTA, COST MP1106 project, and by the Engineering and Physical Sciences Research Council, UK, grant EP/D077869/1, CoWet project, EU.

References

[1] Starov VM, Velarde MG, Radke C. Wetting and spreading dynamics. Surfactant science series, 138. Taylor & Frances; 2008.
[2] Deryaguin BV, Churaev NV, Muller VM. Surface forces. Consultants Bureau, Plenum Press; 1987.
[3] Israelachvili JN. Intermolecular and surface forces. 3rd ed. Academic Press; 2011.
[4] Russel WB, Saville DA, Schowalter WR. Colloidal dispersions. Cambridge University Press; 1999.
[5] Exerowa D, Kruglyakov P. Foam and foam films: theory, experiment, application. Elsevier; 1998.
[6] Churaev NV. Adv Colloid Interf Sci 2003;103:197.
[7] Starov VM, Velarde MG. J Phys Condens Matter 2009;21:464121.
[8] Mechkov S, Cazabat AM, Oshanin G. J Phys Condens Matter 2009;21:464131.
[9] Liang ZP, Wang XD, Lee DJ, Peng XF, Su A. J Phys Condens Matter 2009;21:464117.
[10] Popescu MN, Oshanin G, Dietrich S, Cazabat AM. J Phys Condens Matter 2012;24:243102.
[11] Starov V. Colloid Polym Sci 2013;291:261–70.
[12] Zorin ZM, Churaev NV, Cololid J. USSR Acad Sci 1968;30:371 (in Russian).
[13] Deryagin BV, Ershova IG, Churaev NV. Dokl Akad Nauk SSSR 1968;182:368 [in Russian].
[14] Viktorina MM, Deryagin BV, Ershova IG. Churaev NV. Dokl Akad Nauk SSSR 1971;200:1306 (in Russian).
[15] Mack GL. J Phys Chem 1936;40(2):159.
[16] Veselovsky VS, Pertsev VN. J Phys Chem (USSR Acad Sci) 1936;8(2):245 [in Russian].
[17] Amirfazli A, Hänig S, Müller A, Neumann AW. Langmuir 2000;16:2024–31.
[18] Ajaev VS, Gambaryan-Roisman T, Stephan P. J Colloid Interface Sci 2010;342:550.
[19] Rednikov AY, Colinet P. Langmuir 2011;27:1758.
[20] Deegan RD. Phys Rev E 2000;61:475.
[21] Deegan RD, Bakajin O, Dupont TF, Huber G, Nagel SR, Witten TA. Phys Rev E 2000;62:756.
[22] Moosman S, Homsy GM. J Colloid Interface Sci 1980;73:212.
[23] Eggers J, Pismen LM. Phys Fluids 2010;22:112101.
[24] Potash Jr M, Wayner Jr PC. Int J Heat Mass Transfer 1972;15:1851.
[25] Ajaev VS, Homsy GM, Morris SJS. J Coll Int Sci 2002;254:346–54.
[26] Girard F, Antoni M, Sefiane K. Langmuir 2008;24:9207.
[27] Picknett RG, Bexon R. J Colloid Interface Sci 1977;61:336.
[28] Girard F, Antoni M, Faure S, Steinchen A. Langmuir 2006;22:11085.
[29] Girard F, Antoni M, Faure S, Steinchen A. Microgravity Sci Technol 2006;XVIII-3/4:42.
[30] Girard F, Antoni M, Faure S, Steinchen A. Colloid Surf A 2008;323:36.
[31] Girard F, Antoni M. Langmuir 2008;24:11342.
[32] Semenov S, Starov VM, Rubio RG, Velarde MG. Colloid Surf A 2010;372:127.

[33] Hu H, Larson RG. J Phys Chem B 2002;106:1334.
[34] Guena G, Poulard C, Voue M, Coninck JD, Cazabat AM. Colloid Surf A 2006;291:191.
[35] Dunn GJ, Wilson SK, Duffy BR, David S, Sefiane K. J Fluid Mech 2009;623:329.
[36] David S, Sefiane K, Tadrist L. Colloid Surf A 2007;298:108.
[37] Schonfeld F, Graf KH, Hardt S, Butt HJ. Int J Heat Mass Transfer 2008;51:3696.
[38] Bhardwaj R, Fang X, Attinger D. New J Phys 2009;11:075020.
[39] Starov VM, Sefiane K. Colloid Surf A 2009;333:170.
[40] Lee KS, Cheah CY, Copleston RJ, Starov VM, Sefiane K. Colloid Surf A 2008;323:63.
[41] Starov VM, Kostvintsev SR, Sobolev VD, Velarde MG, Zhdanov SA. J Colloid Interface Sci 2002;252:397.
[42] Starov VM, Kostvintsev SR, Sobolev VD, Velarde MG, Zhdanov SA. J Colloid Interface Sci 2002;246:372.
[43] Semenov S, Starov VM, Rubio RG, Agogo H, Velarde MG. Colloid Surf A 2011;391:135.
[44] Sobac B, Brutin D. Langmuir 2011;27:14999.
[45] Semenov S, Starov VM, Velarde M, Rubio RG. Eur Phys J Spec Top 2011;197:265.
[46] Semenov S, Starov VM, Rubiob RG, Velarde M. Langmuir 2012;28:15203.
[47] Doganci MD, Sesli BU, Erbil HY. J Colloid Interface Sci 2011;362:524.
[48] Semenov S, Trybala A, Agogo H, Kovalchuk N, Ortega F, Rubio RG, et al. Langmuir 2013;29:10028.
[49] Trybala A, Okoye A, Semenov S, Agogo H, Rubio RG, Ortega F, et al. J Colloid Interf Sci 2013;403:49.
[50] Murisic N, Kondic L. J Fluid Mech 2011;679:219.
[51] Mattia D, Rossi MP, Kim BM, Korneva G, Bau HH, Gogotsi Y. J Phys Chem B 2006;110:9850.
[52] Sefiane K. Adv Colloid Interface Sci 2014;206:372–81.
[53] Popov YuO. Phys Rev E 2005;71:036313.
[54] Venzmer J. COCIS 2011;16:335–43.
[55] Starov V, Ivanova N, Rubio RG. Adv Colloid Interface Sci 2010;161:153–62.
[56] Karapetsas G, Craster RV, Matar OK. J Fluid Mech 2011;670:5–37.
[57] Maldarelli C. J Fluid Mech 2011;670:1–4.
[58] Ritacco H, Ortega F, Rubio RG, Ivanova N, Starov VM. Colloid Surf A 2010;365:199.
[59] Ivanova N, Starov VM, Johnson D, Hilal N, Rubio RG. Langmuir 2009;25:3564.
[60] Svitova T, Hill RM, Radke CJ. Colloid Surf A 2001;183–185:607.
[61] Wagner R, Richter L, Weißmuller J, Reiners J, Klein KD, Schaefer D, et al. Appl Organomet Chem 1997;11:617.
[62] Ivanova N, Starov VM, Rubio RG, Ritacco H, Hilal N, Johnson D. Colloid Surf A 2010;354:143.